Electrostatics of DNA Complexes with Cationic Lipid Membranes

A. G. Cherstvy*

Max-Planck-Institut für Physik Komplexer Systeme, Nöthnitzer Strasse 38, 01187 Dresden, Germany

Received: January 2, 2007; In Final Form: April 12, 2007

We present the exact solutions of the linear Poisson−Boltzmann equation for several problems relevant to electrostatics of DNA complexes with cationic lipids. We calculate the electrostatic potential and electrostatic energy for lamellar and inverted hexagonal phases, concentrating on the effects of dielectric boundaries. We compare our results for the complex energy with the known results of numerical solution of the nonlinear Poisson−Boltzmann equation. Using the solution for the lamellar phase, we calculate the compressibility modulus and compare our findings with the experimental data available. Also, we treat charge−charge interactions across, along, and between two low-dielectric membranes. We obtain an estimate for the strength of electrostatic interactions of one-dimensional DNA smectic layers across the lipid membrane. We discuss in the end some aspects of two-dimensional DNA condensation and DNA−DNA attraction in the DNA−lipid lamellar phase in the presence of di- and trivalent cations. We analyze the equilibrium DNA−DNA separations in lamellar complexes using the recently developed theory of electrostatic interactions of DNA helical charge motifs.

1. Introduction

1.1. DNA−CL Complexes: Experimental Observations. Complexes of DNA with cationic lipids (CLs), lipoplexes, are promising nonviral transfection vectors for gene therapy applications.[1] Self-assembly of lipid membranes composed of cationic and neutral lipids with relatively rigid oppositely charged biomacromolecules has been studied experimentally, in particular for DNA,[2−11] F-actin,[12] microtubules,[13] and some highly charged filamentous viruses.[12] Complexation, morphology, and phase behavior of resulting complexes are believed to be governed to a large extent by the ratio of surface charge densities of the two complexing species. For F-actin, for instance, the unit cell of the lamellar-stack complexes consists of two layers of F-actin on both sides of the membrane due to a mismatch in their surface charge densities.[12] For DNA, several morphologies of complexes with CL membranes have been detected, the more commonly observed lamellar L_α^c and inverted hexagonal H_{II}^c phase being the most known examples.[2,3] Lamellar DNA−CL complexes consist of one-dimensional (1D) DNA monolayers with a well-defined DNA−DNA separation, which are sandwiched between the CL bilayers.[2] The dominant interactions in the complexes are electrostatic because of huge charge densities of the complexing species: The surface area per lipid molecule is ∼70 Å^2; the area per phosphate on B-DNA surface is ∼100 Å^2.[14] The DNAs in the lattice were shown to be correlated both in the DNA layer plane and across the lamellar stack.[4] In the inverted hexagonal DNA−CL phase, DNA rods are surrounded by a water cylindrical shell with lipid monolayers wrapped around it forming inverted cylindrical micelles (honeycomb structure).[3]

The mixing of DNAs and CLs results in their spontaneous self-assembly into ∼0.2-μm-sized particles of DNA−CL complexes.[1] DNA−CL lamellar and inverted hexagonal complexes are stabilized by electrostatic attraction between negatively charged DNA and positively charged CLs. The electrostatic repulsion between DNAs in DNA layers and between lipid monolayers across the aqueous interlayer tend on the contrary to destabilize the DNA−CL lamellar assembly, especially at low salt concentrations. In the inverted hexagonal phase, attractive electrostatic interactions of DNAs with the lipid membranes are expected to be stronger than those in the lamellar phase, because the opposite charges of DNAs and of lipids are in better contact. This electrostatic driving force for $L_\alpha^c \rightarrow H_{II}^c$ phase transition is opposed by the membrane elastic deformations. The cost of these deformations is reduced by lowering the membrane bending elasticity via adding the cosurfactant molecule hexanol (membrane bending rigidity drops from $\sim 20 k_B T$ down to $2-5 k_B T$).[3] DNA−CL complexes adapt H_{II}^c morphology if the membrane charge density is lower than some critical value because there is an electrostatic penalty connected with bending/wrapping of a charged membrane that grows with the surface charge density. The second pathway for $L_\alpha^c \rightarrow H_{II}^c$ transition is the mechanical one—a spontaneous negative membrane curvature is introduced via addition of helper 1,2-dioleoylglucerophosphatidylethanolamine (DOPE) lipids, which are capable of forming inverted hexagonal phases in the absence of DNA.[3]

Another widely accepted explanation for DNA−CL complexation and lipoplex stability is the entropic mechanism—the release of condensed counterions from DNAs and from CLs. This release has been shown to be maximal and nearly complete at the isoelectric point of the complexes.[7,15] In the bulk solution, the cations are accumulated in the vicinity of highly charged DNA molecules and on lipid membranes—counterions screen the electrostatic fields and reduce the electrostatic energy of the system. Being mixed together, DNAs and CLs form complexes and bring their counterions with them. However, these condensed counterions are no longer needed to screen the interactions inside the complexes—mobile CLs on membranes are now in contact with the negative DNA charges and can screen electrostatic interactions. Thus, the condensed counterions

* Author to whom correspondence should be addressed. E-mail: cherstvy@pks.mpg.de.

10.1021/jp0700175 CCC: $37.00
Published on Web 06/16/2007

are released into the bulk solution, gaining additional translational entropy of $\sim k_B T$ per released counterion.[5]

DNA−CL lamellar and inverted hexagonal structures have been studied by high-resolution synchrotron X-ray diffraction.[2−4] In lamellar complexes, the separation between DNAs in the layer increases from $h \approx 24$ to 57 Å with decreasing membrane charge density (with the DNA axes across the lamellar stacks often positioned on a nearly hexagonal lattice). The latter is controlled by the ratio/composition of positively charged 2,3-dioleyloxypropyltrimethylammonium chloride (DOTAP) and neutral/helper 1,2-dioleoylglucerophosphatidylcholine (DOPC) lipids. For membranes with a lower charge density, the lamellar structures cease to be stable. (Excess neutral lipids demix from the complexes, and the membranes' stability is probably decreased at large DNA−DNA separations in the complexes.) The observed DNA−DNA separations fit the picture of electroneutral counterion-free DNA−CL complexes—DNA charges totally balance the lipid charges, which have been suggested to be most stable[2] due to a maximal counterion release. In excess of CLs, however, a positively charged DNA−CL assembly is a stable state, whereas in excess of DNA the negatively overcharged aggregates are stable (coexisting with excess lipids or DNAs in solution); see discussion in ref 16. It was shown that the distances between DNAs in isoelectric DNA−CL lamellar complexes decrease slightly as the concentration of monovalent salt in solution n_0 increases.[5] The separation between opposing lipid monolayers in DNA−CL lamellar complexes—the thickness of the water gap—was shown to stay typically constant at ∼25 Å, which fits the B-DNA with its first hydration layer. The thickness of the membranes used is ∼40 Å, depending however slightly on the lipid composition. (Neutral colipids used are shorter than CLs.[5]) For the inverted hexagonal phase, the X-ray diffraction data show that the water cylinders are ∼24−28 Å in diameter.[3]

1.2. DNA−CL Complexes: Theoretical Studies. Thermodynamic behavior of lamellar DNA−CL complexes was first studied theoretically in refs 17 and 18 on the basis of the nonlinear Poisson−Boltzmann (PB) theory. Electrostatic screened interactions of surface charges on DNA (modeled as a homogeneously charged rod) and on the CL membranes, the entropy change of mobile ions inside the complexes as compared to their entropy in solution, and the (ideal) mixing entropy of membrane lipids with a possibility of adjustment of their distributions to that of DNA lattice have been taken into account. Numerical optimization of the free energy functional has shown that the total free energy is always minimal for the complexes close to electroneutrality. As a result of self-consistent free energy calculations, the profile of mobile CLs that accumulate in the vicinity of DNA for weakly charged membranes has been calculated. It was shown that these charge modulations substantially decrease the free energy of the complex. Electrostatically induced undulations of the lipid membrane in lamellar complexes have also been studied with the conclusion that the corrugation amplitude increases for larger DNA−DNA separations (it reaches up to several ångstroms) and for softer membranes.[19,20]

Phase behavior and coexistence of different phases of DNA−CL complexes have been studied later in ref 18. The preferred equilibrium geometry of the complexes—lamellar, inverse hexagonal, free DNA, or DNA-free lamellar—was shown to be governed by (a subtle) interplay of the ratio of charged/neutral lipids, the charge ratio of membranes to DNAs, the membrane bending elasticity, and the mixing entropy of lipids, as follows from the minimization of electrostatic, elastic, and mixing free energy contributions in the model;[18] see also ref 10. Thus, the complicated problem of equilibrium adsorption of DNA rods from electrolyte solution into DNA−CL complexes of different morphologies has been solved self-consistently in ref 18. It was shown that for soft membranes the inverted hexagonal phase is preferred over the lamellar phase for fractions of cationic lipids $\phi_C \lesssim 0.5$; see Figure 6 in ref 18. Also, due to a possibility to adjust the DNA−DNA separations, the lamellar phase can tolerate larger changes in the lipid composition as compared to the inverted hexagonal phase.

Although working within a more accurate nonlinear PB theory in the cell model, the authors of refs 17 and 18 have not considered the effects of the dielectric boundaries (DNA−water and membrane−water); they presented no analytic solutions for the complex (formation) energy and for the strength of interaction of DNA rods across and along the lipid membrane and also included no effects of DNA charge helicity in their model. The latter in particular appear to be crucial for description of two-dimensional (2D) DNA condensation in lamellar DNA−CL complexes with multivalent cations,[9] as we show in the last section of the paper. We consider all of these issues in the present paper, however in a more crude, linear PB approximation.

DNA has been modeled as a homogeneously charged rod also in other papers on DNA−CL lamellar complexes with the conclusion of purely repulsive rod−rod interactions in such systems.[21−24] In ref 21, for instance, the repulsion electrostatic energy of the two rods confined between low-dielectric membranes with the mobile surface charges was shown to decay as $\propto 1/h$ with the rod−rod separation. This particular nonlinear-PB-equation-based model is however valid only when DNA−DNA spacings are much larger than separations between membranes and for vanishingly small n_0. Experimentally measured compressibility modulus of DNA−CL lamellar stack B was shown to be consistent with $1/h$ power-law decay,[5] while exponentially screened DNA−DNA electrostatic or hydration repulsions do not reveal good agreement with the data. The revised analysis of $B(h)$ data on the basis of the theory of refs 17 and 18 has however led to conclusion that at $h < 33$ Å the hydration DNA−DNA repulsion dominates whereas for larger separations the electrostatics is more important.[25] We address the dependence of B on the density of the DNA lattice in subsection 3.3.

Recently, some Monte Carlo computer simulations of self-assembly of DNA rods with oppositely charged CLs have been performed in a salt-free regime on the basis of "water-free" coarse-grained models.[23,24] The existence of the DNA−CL lamellar phase has been predicted, and its thermodynamic stability has been confirmed. In accordance with experiments, in the lamellar phase the charge density of the DNA layer was shown to match closely the charge density of lipids assembled into bilayers on both sides of the DNA layer. Theoretically predicted charge density modulations on the lipid membranes[17,18] that occur to improve the matching between charge density of DNA lattice and that of sandwiching membranes have also been confirmed to take place in simulations.[24] It has also been shown that at higher membrane charge densities (high fraction of CLs) the formation of pores in the membrane is enhanced. It was suggested that DNAs can pass through these holes and leave the complex, thereby contributing to a higher transfection efficiency of the DNA−CL lamellar complexes at higher membrane charge densities observed in the clinical studies.[1] Note however that the potentials used in these computer simulations studies for charge−charge interactions do not include the effects of electrostatic screening by electrolyte and of the membrane low-dielectric interior.

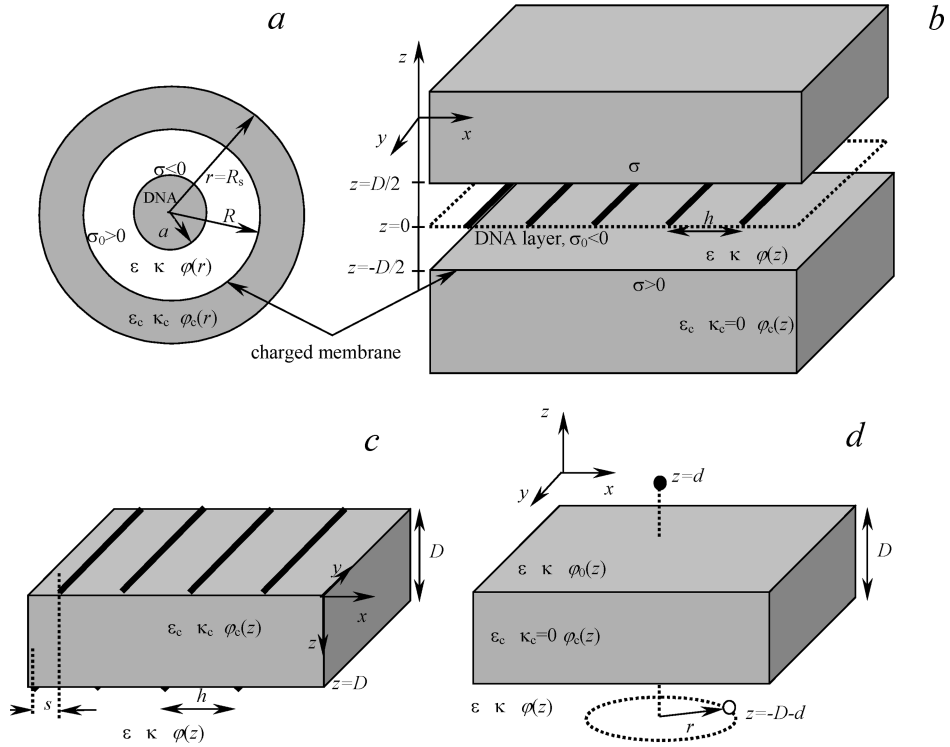

Figure 1. (a) Cylindrical cell model as a model representation of the inverse hexagonal DNA−CL phase. (b) Stack of oppositely charged strings between two low-dielectric half-spaces as a model for DNA−CL lamellar complexes. (c) The model of interaction of two DNA string layers across the low-dielectric membrane of thickness *D*. (d) Interaction of two charges across a low-dielectric membrane.

Bruinsma has shown recently that isoelectric lamellar DNA−CL complexes are unstable with respect to adsorption of both additional DNA strands and CLs.[15] Entropically driven release of condensed counterions from the adsorbing species was shown to be the reason for this counterintuitive statement. Experimental hint for this prediction is a rapid increase of equilibrium DNA−DNA separations in the DNA−CL lamellar phase upon approach to the isoelectric point.[5] The limit of no salt and of large Chapman lengths (weakly charged lipid layers) has only been considered in this paper, and the effects of low-dielectric boundaries have been neglected.

The degree of correlations of DNAs both along and across the lamellar stack of DNA−CL complexes have been measured experimentally;[5] theoretical understanding of DNA correlations in neighboring stacks of lamellar complexes is however still not complete. The existence of sliding columnar DNA−CL phases for instance has been predicted theoretically, implying long-ranged orientational correlations of DNAs in the neighboring layers but no DNA positional correlations.[26] Several mechanisms exist for description of DNA−DNA interactions and correlations across the lipid membrane in DNA−CL lamellar complexes;[27−29] they include both membrane elastic deformations in neighboring layers and electrostatics of rod−rod interactions.[30] We address similar problems in subsection 4.4, calculating the strength of electrostatic interactions of two layers of charged strings across a low-dielectric membrane.

1.3. DNA−CL Lamellar Complexes: 2D DNA Condensation. The picture DNA−CL self-assembly becomes more complicated when some di- and trivalent cations common in cells (Mn^{2+}, Mg^{2+}, Co^{2+}, spermine^{4+}, and spermidine^{3+}) are added into the solution: 2D DNA condensation in lamellar DNA−CL complexes takes place.[9] Namely, above a critical concentration of divalent cations used, ∼0.01−0.05 M, and growing as the membranes become less and less charged, an abrupt change of DNA−DNA separations from $h_{eq} \approx 45-50$ Å to $h_{eq} \approx 28-30$ Å has been detected in experiments.[9] This indicates a change from repulsive to attractive interactions between DNA molecules in the complexes at this critical salt concentration. This separation drop contradicts the picture of isoelectric DNA−CL complexes and the predictions of existing theories of DNA−CL complexes. We show in the last section that the helicity of DNA charge distribution, neglected in theoretical models published previously, can lead to this DNA−DNA attractive behavior.

Although some of these cations are capable of affecting the membrane elastic and electrostatic properties,[10] more likely they modify electrostatic DNA−DNA forces in the lamellar assembly. It has been shown that in solutions of Co^{2+} the fraction $\theta \approx 0.63$ of DNA charge is neutralized by divalent cations that are trapped inside the complexes,[9] while fractions $\theta \approx 0.8-0.9$ are needed to trigger the DNA condensation in three dimensions.[31] In dense columnar hexagonal DNA lattices under osmotic stress, the presence of the same specific cations in solution also triggers DNA condensation.[32,33] Attractive force between DNA molecules exists in 3D dense hexagonal phases at DNA−DNA intermolecular separations of $h \approx 28-32$ Å, which is close to h_{eq} in 2D condensed lamellar complexes.[9]

Below, we often neglect fine molecular details of DNA and consider it as a uniformly charged rod, studying the inverse hexagonal phase, or as a charged thin string in the content of the lamellar DNA−CL phase. The treatment of 2D DNA condensation[9] might however require more detailed models for DNA charges—helical charge motifs. It would be desirable to develop a theory of electrostatic interactions of DNA double spirals in DNA−CL complexes. In electrolyte solution, the problem of electrostatic interactions of two parallel duplexes has recently been solved within linear PB theory;[34] see also refs 35−45. It is a complicated task to obtain similar expressions for interactions of charged helices close to or between low-dielectric membranes. That is beyond the scope of the current paper and can be a task for future research.

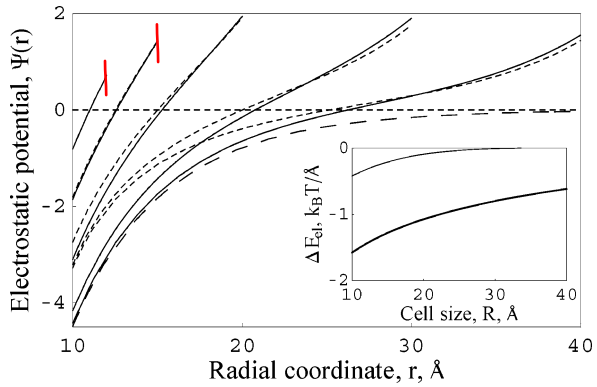

Figure 2. Distribution of the electrostatic potential in the cylindrical cell model for isoelectric inverted hexagonal DNA−CL complexes. Parameters: $R = 12$, 15, 20, 30, 40 Å (from left to right), $\kappa^{-1} = 7$ Å, $\kappa_c = 0$, $\xi = \xi_0 = 4.2$, $a = 10$ Å, $\epsilon_c = 2$, $\epsilon = 80$. The dotted curves are the numerical solutions of the nonlinear PB equation for the same parameters but for $\epsilon_c/\epsilon = 0$; the dashed curve is for $\Psi_0(r)$. The inset shows the complex electrostatic formation energy, eq 6, for $\kappa^{-1} = 7$ Å (thin) and $\kappa^{-1} = 60$ Å (solid curve).

We rationalize the recent results on equilibrium DNA−DNA separations in three-dimensional (3D) DNA precipitates with spermine^{4+} based on the existing theory of interaction of DNA charged spirals in electrolytes and discuss some implications to 2D DNA condensation. We present also some analytical solutions for the electrostatic interaction of point charges along and across a low-dielectric membrane, subsections 4.1 and 4.2, which might be helpful to treat the problem of duplex−duplex electrostatic interaction in DNA−CL complexes in the future.

The paper is structured as follows. We obtain the electrostatic potential and energy in the inverse hexagonal and lamellar phases in sections 2 and 3. We calculate the compressibility modulus of the lamellar phase as a function of separation between DNAs in a 1D DNA stack, subsection 3.3. We discuss some aspects of electrostatic interactions of charges across, along, and between low-dielectric membranes, subsection 4.1. We calculate the electrostatic interaction energy of two arrays of charged strings across a low-dielectric membrane in subsection 4.4. We present some results on properties of electrostatic interactions of DNA spirals that can be relevant to 2D DNA condensation in DNA−CL complexes with specific multivalent cations, section 5. In all sections we work within the linearized PB theory and treat the effects of low-dielectric boundaries explicitly.

2. Inverted Hexagonal Phase

2.1. Electrostatic Potential. We calculate below the distribution of the dimensionless electrostatic potential $\Psi = e_0\varphi/(k_BT)$ and the excess rod electrostatic energy ΔE_{el} in the cylindrical cell model. This is a simple model for the DNA−CL inverted hexagonal phase: The water cylinders with DNA molecules inside are surrounded by a low-dielectric membrane. The DNA is modeled as a uniformly negatively charged rod of radius a, which is surrounded by a cylindrical shell of radius R with electrolyte solution with the Debye screening length $1/\kappa$ and with the dielectric constant $\epsilon = 80$. This shell is surrounded by a shell of low-dielectric medium, with the dielectric constant ϵ_c and radius R_s, mimicking the lipid membrane embracing DNA rods in this phase. (The membrane thickness is set to ≈ 40 Å, Figure 1a.) For generality of calculations, we set a nonzero value of $1/\kappa_c$. The DNA rod linear charge density is $1/b$ whereas that of positively charged lipid membrane cylinder is $1/b_0$. That results in Manning's parameter $\xi = l_B/b$ for the DNA rod and $\xi_0 = l_B/b_0$ for the lipid cylinder; the corresponding surface charge densities are $\sigma = -e_0/(2\pi ab) < 0$ and $\sigma_0 = e_0/(2\pi ab_0) > 0$, where $e_0 > 0$ is the elementary charge. Here, the Bjerrum length in water at the room temperature is $l_B = e_0^2/(\epsilon k_BT) \approx 7$ Å.

The linear PB equation

$$\frac{\partial^2\Psi(r)}{\partial r^2} + \frac{1}{r}\frac{\partial\Psi(r)}{\partial r} = \kappa^2\Psi(r) \tag{1}$$

has been solved in the cylindrical cell model together with the boundary conditions at the rod surface $a(\partial\Psi(r)/\partial r)|_{r=a} = 2\xi$ on the water−lipid interface $R((\partial\Psi(r)/\partial r) - (\epsilon_c/\epsilon)(\partial\Psi_c(r)/\partial r))|_{r=R} = 2\xi_0$ and at the cell boundary $(\partial\Psi_c(r)/\partial r)|_{r=R_s} = 0$. Here $\Psi(r)$ is the potential in the aqueous phase ($a < r < R$), and $\Psi_c(r)$ is the potential in the low-dielectric phase ($R < r < R_s$). Potential inside the rod is constant. Here $\kappa = \sqrt{8\pi l_B n_0}$ is the reciprocal Debye screening length of a 1:1 electrolyte solution.

The solution for the potential as a function of the distance from the rod axis r is

$$\Psi(r) = \alpha K_0(\kappa r) + \beta I_0(\kappa r) \quad \Psi_c(r) = \gamma K_0(\kappa_c r) + \delta I_0(\kappa_c r) \tag{2}$$

where the coefficients are

$$\alpha = A_4\left[-\frac{2\xi_0}{\kappa R}I_1(\kappa a) + \frac{2\xi}{\kappa a}\left(I_1(\kappa R) - \frac{\kappa_c\epsilon_c}{\kappa\epsilon}\frac{A_3}{A_4}I_0(\kappa R)\right)\right]\Bigg/ \left(A_1A_4 + A_2A_3\frac{\kappa_c\epsilon_c}{\kappa\epsilon}\right)$$

$$\beta = \frac{2\xi}{\kappa a I_1(\kappa a)} + \alpha\frac{K_1(\kappa a)}{I_1(\kappa a)}$$

$$\gamma = \frac{I_1(\kappa_c R_s)[\alpha K_0(\kappa R) + \beta I_0(\kappa R)]}{A_4}$$

$$\delta = \gamma\frac{K_1(\kappa_c R_s)}{I_1(\kappa_c R_s)} \tag{3}$$

and $A_1 = K_1(\kappa R)I_1(\kappa a) - K_1(\kappa a)I_1(\kappa R)$, $A_2 = K_0(\kappa R)I_1(\kappa a) + K_1(\kappa a)I_0(\kappa R)$, $A_3 = I_1(\kappa_c R)K_1(\kappa_c R_s) - K_1(\kappa_c R)I_1(\kappa_c R_s)$, and $A_4 = I_1(\kappa_c R_s)K_0(\kappa_c R) + I_0(\kappa_c R)K_1(\kappa_c R_s)$. Here $I_n(x)$ and $K_n(x)$ are the modified Bessel functions of the nth order. The solution for $\Psi(r)$ is plotted in Figure 2 as solid curves for the isoelectric inverted hexagonal complexes. If one neglects the potential variation inside the low-dielectric phase and sets $\kappa_c = 0$, then the potential in aqueous solution becomes

$$\Psi(r) = \frac{2\xi_0\kappa a[I_1(\kappa a)K_0(\kappa r) + K_1(\kappa a)I_0(\kappa r)] - 2\xi\kappa R[I_1(\kappa R)K_0(\kappa r) + K_1(\kappa R)I_0(\kappa r)]}{\kappa a\kappa R[K_1(\kappa a)I_1(\kappa R) - I_1(\kappa a)K_1(\kappa R)]} \tag{4}$$

which appears to be very close to the results of eq 2 for the typical parameter values used. For large cell radii, this potential turns into the electrostatic potential of a single uniformly charged rod

$$\Psi_0(r) = -\frac{2\xi K_0(\kappa r)}{\kappa a K_1(\kappa a)} \tag{5}$$

The linearized PB theory used throughout this paper is applicable strictly speaking for weak electrostatic potentials, $|\Psi|$

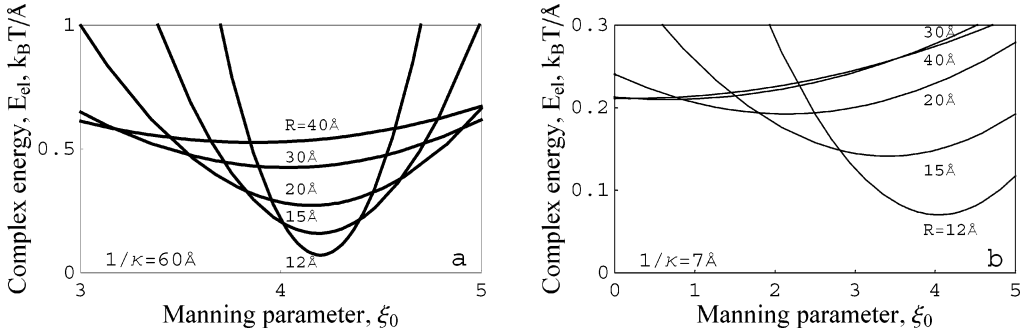

Figure 3. Electrostatic energy of inverted hexagonal complexes as a function of the lipid membrane charge density. Parameters are the same as in Figure 2.

$\ll 1$. In Figures 2 and 3 we however use the DNA bare charge density (no counterions condensed) $-e_0/1.7$ Å along the axis, i.e., $\xi \approx 4.2$. That results in a high electrostatic potential close to the rod surface and thus violates the requirements for the linear theory. For comparison, in Figure 2 as dotted curves we show the solutions of the nonlinear PB equation in the cell model (with $\kappa^2 \sinh \Psi$ in the right-hand side of eq 1) for the same ionic strengths and at $\epsilon_c/\epsilon = 0$. For small cell radii, where $|\Psi|$ is smaller than unity, the results of both linear and nonlinear treatments almost coincide. For larger cells, when the rod surface potential becomes larger than unity, the nonlinear theory results in slightly smaller values of $\Psi(a)$ while the general shape of the potential distribution remains quite similar. We do not discuss further in the paper the regimes of applicability of the linear PB equation to highly charged polyelectrolyte systems in general and to electrostatics of DNA−CL complexes in particular. (There exist a number of papers of this subject.) Although both DNA and CLs are highly charged, some tendencies predicted here and below for their complexes from the linear theory can still capture the underlying physics correctly. In general, for the hexagonal assembly of DNA rods well-neutralized by condensed counterions the linearized and nonlinear PB equations in the cylindrical cell model give close results; see, for instance, ref 37.

2.2. Electrostatic Energy. The complex electrostatic energy E_{el} and formation energy $\Delta E_{el}(R)$ can be expressed via the rod and shell surface potentials as (per unit length)

$$E_{el} = \frac{k_B T}{4\pi l_B}\{-\xi\Psi(a) + \xi_0\Psi(R)\} \quad \text{and}$$

$$\Delta E_{el}(R) = E_{el}(R) - E_{el}(\infty) \quad (6)$$

As one could expect, at low salt concentrations the electroneutral complexes are favored, with the Manning parameter for the lipid shell close to that of the DNA, $\xi_0 \approx 4.2$, Figure 3a, calculated per one ångstrom along the cell cylinder. The position of the energy minimum moves progressively toward smaller ξ_0 values away from the isoelectric point as the cell radius grows; the mutual electrostatic coupling of the positively charged lipid shell with the negatively charged DNA rod becomes progressively screened. The complex energy at optimal ξ increases as the thickness of the water shell grows, Figure 3. These tendencies as well as the absolute values of the energy obtained are in qualitative agreement with the results presented in Figure 2 of ref 18, where the free energies of the full nonlinear PB equation and within the model with the mobile membrane lipids have been calculated. At higher n_0 values, the shift of the energy minimum from the isoelectric point is more pronounced, Figure 3b. The steepness of $E_{el}(\xi)$ − parabola increases for denser lattices, similar to Figure 2 of the numerical study of ref 18 (see also the discussion in subsection 3.2 where similar tendencies are predicted for the lamellar complexes).

For electroneutral complexes, the electrostatic potential on the rod surface and on the lipid membrane surface decreases in absolute values as the cell radius R_s decreases, Figure 2. Thus, the complex formation energy ΔE_{el}, being proportional to the difference of surface potentials on DNA and on the membrane in complexes and in a free state, is negative and becomes (exponentially) larger in absolute values for denser assemblies, the inset in Figure 2.[46]

3. Lamellar Phase

3.1. Potential Distribution. In the lamellar DNA−CL phase, the 1D planar layer of well-ordered DNA molecules with DNA−DNA separation h is intercalated between two oppositely charged lipid layers separated by the distance D. We model this system as a perfect array of infinitely thin negatively charged strings (with the net surface charge density $\sigma_0 < 0$) between two positively homogeneously charged planes with charge density $\sigma > 0$, Figure 1b. The dielectric constant in aqueous solution between the planes is $\epsilon = 80$; semi-infinite low-dielectric media have the dielectric constant ϵ_c and contain no mobile charges, $\kappa_c = 0$. Coordinate z is across the stack, x is perpendicular to the strings and along the layer, and y is along the strings. No fluctuation-induced undulations of DNA strings and of the membranes are taken into account below. Also, the lipids on the membrane are treated as immobile, and thus no adjustment of the membrane charge density to that of the DNA lattice is considered, i.e., $\sigma(x) =$ constant.

The potential variation is calculated via solving the Laplace equation in the low-dielectric media and the linear PB equation in the aqueous phase, $\Delta\varphi_c(x,z) = 0$ and $\Delta\varphi(x,z) = \kappa^2\varphi(x,z)$ with $\sigma(x,z) = \sigma[\delta(z - D/2) + \delta(z + D/2)] + \sigma_0 h\delta(z)\sum_j \delta(x - jh)$. We use the Fourier transformation over x for the electrostatic potentials and charge densities

$$\tilde{\varphi}_n(z) = \frac{1}{h}\int_{-h/2}^{h/2} dx\, e^{ingx}\varphi(x,z), \quad \varphi(x,z) = \sum_{n=-\infty}^{\infty} e^{-ingx}\tilde{\varphi}_n(z) \quad (7)$$

where $g = 2\pi/h$. Recently, a similar technique has been used for studying the complex formation of oppositely charged polyelectrolytes,[47−49] the electrostatics of DNA conformational transitions,[41,50] and electrostatics of ion channels and pores.[51] For the Fourier components $\tilde{\varphi}_{n,c}(z)|_{D/2} = \tilde{\varphi}_n(z)|_{D/2}$, $[\epsilon(d\tilde{\varphi}_n(z)/dz) - \epsilon_c(d\tilde{\varphi}_{n,c}(z)/dz)]_{D/2} = 4\pi\sigma\delta_{n,0}$, and $\epsilon(d\tilde{\varphi}_n(z)/dz)|_{z=0} =$

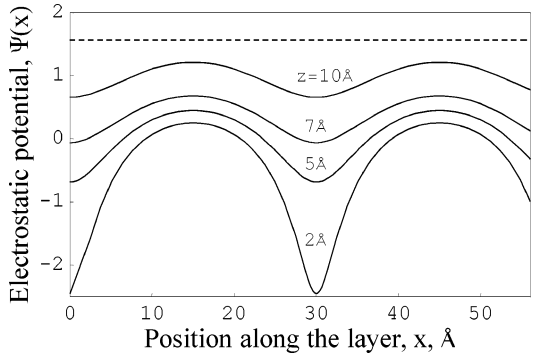

Figure 4. Potential variation from the layer of strings between oppositely charged surfaces for different *z* values. Two periods over *x* are shown. The dotted line is Ψ_{pl}. Parameters: $D = 20$ Å, $1/\kappa = 7$ Å, $h = 30$ Å, $\sigma_0 = -e_0/200$ Å^2, $\sigma = -\sigma_0/2$, $\epsilon_c/\epsilon = 2/80$.

$-2\pi\sigma_0$, where $\delta_{n,0}$ is the Kronecker symbol. Then, the electrostatic potential in the aqueous medium at $z > 0$ is

$$\varphi(x,z) = \frac{4\pi}{\epsilon\kappa}\left\{\frac{\sigma\cosh[\kappa z] + \sigma_0\cosh[\kappa(D/2 - z)]/2}{\sinh[\kappa D/2]} + \sum_{n=1}^{\infty}\cos[ngx]\frac{\kappa\sigma_0}{\kappa_n}\frac{\eta_n\sinh[\kappa_n(D/2 - z)] + \cosh[\kappa_n(D/2 - z)]}{\eta_n\cosh[\kappa_n D/2] + \sinh[\kappa_n D/2]}\right\} \quad (8)$$

and in the low-dielectric phase

$$\varphi_c(x,z) = \frac{4\pi}{\epsilon\kappa}\left\{\frac{\sigma_0/2 + \sigma\cosh[\kappa D/2]}{\sinh[\kappa D/2]} + \sum_{n=1}^{\infty}\cos[ngx]\frac{\kappa\sigma_0}{\kappa_n}e^{ng(D/2-z)} \times \frac{e^{-\kappa_n D/2}\{\eta_n\cosh[\kappa_n D/2] + \sinh[\kappa_n D/2]\} + (1 + e^{-\kappa_n D})(1 - \eta_n)/2}{\eta_n\cosh[\kappa_n D/2] + \sinh[\kappa_n D/2]}\right\} \quad (9)$$

where we use the notation $\eta_n = \epsilon_c ng/\epsilon\kappa_n$. Here

$$\kappa_n = \sqrt{\kappa^2 + n^2 g^2} \quad (10)$$

are the modified reciprocal screening lengths. Note that convergence of the series is relatively slow for comparably large κ values when the arguments of the functions used do not change fast with *n*. Note again that the linear PB theory used here applies for weakly charged surfaces only.

The string layer charge density is

$$\sigma_0 = -e_0/(bh) \quad (11)$$

where $b = b_{DNA}/(1 - \theta)$ is the separation between the nearest charges along the string, $b_{DNA} = 1.7$ Å is the average separation between the phosphates along the DNA axis, and θ is the value of DNA charge neutralization by the adsorbed cations. The neutralization fraction of DNA in a 1:1 salt solutions is $\theta \approx 0.8$, as follows from the polyelectrolyte theories.[52]

As one could expect, the potential variations due to discreteness of DNA strands in the layer decay as we move away form the layer of strings, Figure 4, plotted for isoelectric DNA−CL complexes, meaning that $\sigma = -\sigma_0/2$. For the chosen charge densities and screening lengths, the potential stays relatively small for distances $z \gtrsim 3$ Å from the string layer. Potential variations become however larger as κ decreases and electrostatics becomes less screened. At some distance from the strings' layer the average value of the potential becomes positive and for large values of *D* at $z \to D/2$ it approaches the potential of a separated positively charged plane, $\Psi_{pl} = 4\pi\sigma e_0/(\epsilon\kappa k_B T)$, the dotted line in Figure 4. In this figure, the thickness of the water layer was set to $D = 20$ Å, close to the experimentally observed water thicknesses of 25 Å in DNA−CL lamellar phase.[5]

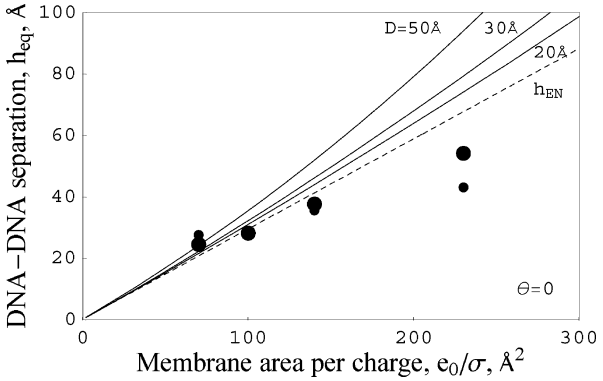

Figure 5. Optimal string−string separation in lamellar complexes for different *D* calculated at $\theta = 0$, $1/\kappa = 60$ Å. Measured DNA−DNA separations in DNA−CL lamellar complexes are large (0 mM of NaCl) and small dots (150 mM of NaCl), as taken from Figures 4a and 4b of ref 11.

3.2. Electrostatic Energy and Equilibrium DNA−DNA Separations. The electrostatic energy of this lamellar phase, the string layer with two neighboring oppositely charged planes, is calculated as

$$E_{el} = \frac{1}{2h}\int_{-h/2}^{h/2} dx \int_{-\infty}^{\infty} dz\, \varphi(x,z)\sigma(x,z) \quad (12)$$

Then (per unit surface area) we obtain

$$E_{el} = \frac{2\pi\sigma_0}{\epsilon\kappa}\left\{\frac{\sigma + \sigma_0\cosh[\kappa D/2]/2}{\sinh[\kappa D/2]} + \sum_{n=1}^{\infty}\frac{\kappa\sigma_0}{\kappa_n}\frac{\eta_n\tanh[\kappa_n D/2] + 1}{\eta_n + \tanh[\kappa_n D/2]}\right\} + \frac{4\pi\sigma}{\epsilon\kappa}\left\{\frac{\sigma\cosh[\kappa D/2] + \sigma_0/2}{\sinh[\kappa D/2]}\right\} \quad (13)$$

Note that as $D \to \infty$ eq 8 turns into the potential created by a separate layer of negatively charged strings in electrolyte solution. Being positioned directly on a uniformly charged plane with the charge density $\sigma > 0$, this layer creates the potential $\varphi(r) = (2\pi/\epsilon\kappa)[(\sigma_0 + \sigma)\, e^{-\kappa z} + 2\sigma_0\sum_{n=1}^{\infty}\cos(ngx)(\kappa\, e^{-\kappa_n z}/\kappa_n)]$ at $z > 0$ and has the electrostatic energy (per unit area)

$$E_{el} = \frac{\pi}{\epsilon\kappa}\left[(\sigma_0 + \sigma)^2 + 2{\sigma_0}^2\sum_{n=1}^{\infty}\frac{\kappa}{\kappa_n}\right] \quad (14)$$

The homogeneous terms in eq 13 for small *D* have a minimum for the electroneutral complexes with equilibrium string−string separation

$$h_{EN} = e_0/(2b\sigma) \quad (15)$$

In general, the equilibrium h_{eq}, as found from the minimum of E_{el} (eq 13), is slightly larger than h_{EN} for typical *D* and κ values used, Figure 5. The deviation of h_{eq} from h_{EN} increases for larger *D* and for larger κ values, when the $\kappa D \ll 1$ assumption is not valid anymore. As the electrostatic influence of positively charged planes onto the negatively charged layer of strings

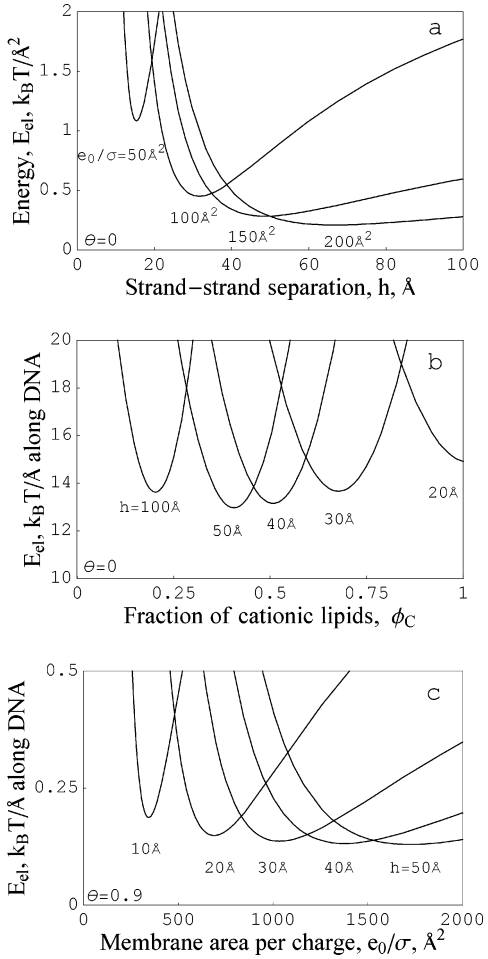

Figure 6. Electrostatic energy of DNA−CL lamellar complexes as a function of (a) DNA−DNA separation h for different values of σ at $\theta = 0$, (b) cationic lipid fraction ϕ_C for different h at $\theta = 0$, and (c) $1/\sigma$ for different h at $\theta = 0.9$. Other parameters: $1/\kappa = 60$ Å, $D = 20$ Å.

decays exponentially, the repulsion between the strings tends to increase the h value.

Experimental data on DNA−DNA separations in isoelectric lamellar DNA−CL complexes as a function of the lipid membrane charge density are plotted in Figure 5 (see Figure 4 of ref 11 for the data on nonelectroneutral complexes as well). The data are in agreement with the predictions of simple isoelectric DNA−membrane charge matching, eq 15, provided no counterions are condensed on DNA. (They all are released, i.e., $b = b_{DNA}$.) The data disagree completely with eq 15 for 80−90% DNA charge compensation (not shown). With increases of n_0, the measured h_{eq} values typically decrease slightly, Figure 5. (Our model predicts however an increase of h_{eq} with κ, presumably because the electrostatics becomes weaker.)

The electrostatic energy variation near h_{eq}, which is always close to electroneutrality for the values of κ chosen, is plotted in Figure 6a. As we move away from the isoelectric point, the unfavorable electrostatic repulsion between the strings in the layer (for denser DNA lattices) or between the membrane planes (for diluted DNA lattices) causes the energy to increase, Figure 6. From eq 13 it follows that for higher membrane charge densities σ the position of the $E_{el}(h)$ minimum moves toward smaller h values, the energy value in the minimum increases, and the steepness of the energy parabola $E_{el}(h)$ near the minimum grows. (Energy per DNA length has similar tendencies, Figure 6a.) The slope of $E_{el}(h)$ dependence for $h < h_{eq}$ is quite similar for all of the membrane charge densities considered. All of these tendencies are in qualitative agreement with Figure 4 of ref 17, where the results of numerical solutions of the nonlinear PB equation for lamellar DNA−CL complexes have been presented.

In Figure 6b, we present the electrostatic energy dependence on the fraction of cationic lipids ϕ_C in the membrane; i.e., the membrane charge density is $\sigma = e_0\phi_C/70$ Å^2. We obtain that the steepness of the $E_{el}(\phi_C)$ parabola near the minima (plotted per unit length of DNA in complexes, i.e., the energy in eq 13 is multiplied by h) increases for larger h_{eq} values. This is similar to the numerical results for $E_{el}(\phi_C)$ dependencies presented in Figure 5 in ref 17, Figure 3 in ref 18, and Figure 2 in ref 19, obtained within a quite different model for DNA−CL complexes. (The nonlinear PB equation has been solved in the cell model for the uniformly charged DNA rod with a radius of 10 Å confined between positively charged membranes; the mobility and adjustment of charges on the membrane have been taken into account.) For larger κ, the $E_{el}(\phi_C)$ energy parabola becomes more shallow (not shown). In Figure 6c, we show $E_{el}(\sigma)$ dependence for different h values calculated at $\theta = 0.9$, the value used also in the next subsection. Both for the inverted hexagonal and lamellar DNA−CL assembly we do not observe a substantial dependence of the complex formation energy on the dielectric constant of the lipid membranes in the relevant range of physical parameters (data not shown).

3.3. Compressibility Modulus. Near the minimum, the shape of $E_{el}(h)$ can be considered as a parabola with the steepness reflecting forces required to remove the system away from the equilibrium state, Figure 6a, and being thus proportional to the compressibility modulus. As one could expect, the steepness increases for complexes with higher net charge densities, where the electrostatic interactions are stronger, consistent with the experimental data on $B(h)$, Figure 7. This tendency is similar to that for the inverted hexagonal complexes, Figure 3.

The compressibility modulus B of lamellar DNA−CL complexes with various DNA densities has been extracted experimentally from the data on the strength of DNA−DNA correlations within the DNA layer.[4,5] The data show that the correlation length ξ_z of DNA fluctuations in the plane of DNA layer increases from ∼100 to ∼200 Å as h_{eq} grows from 27 to 55 Å. The correlation length across the DNA−lipid stack, ξ_y, grows considerably (from ∼15 to 60 Å) upon the same dilution of the DNA lattice, indicating that DNAs become more correlated in neighboring lamellar layers as h_{eq} increases. This interlayer coupling can occur, for instance, due to interactions between DNA molecules in the neighboring layers (subsection 4.4) or due to coupled local elastic deformations of the lipid membranes.[30]

The B value is connected with ξ_z by the following formula[5]

$$B(h) = k_BT(2\pi)^2 2^{-1/3} \xi_z^{2/3} l_p^{-1/3} h^{-7/3} \qquad (16)$$

where $l_p \approx 500$ Å is the B-DNA bending persistence length.[53] We use here the common value for the DNA persistence length at physiological conditions; in the lamellar stack it can however be different.[54] This value has been used in experiments[5] to evaluate the compressibility modulus of the lamellar phase from DNA−DNA correlations. Different l_p values will change of course the B value but not its dependence on the density of DNA lattice; that is the basic focus of this section. B is also proportional to the energy required for 1D compression of the DNA stack. Let us attribute the measured B values purely to

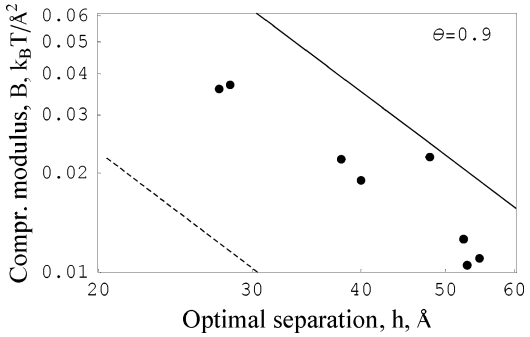

Figure 7. Compressibility modulus of DNA−CL lamellar phase as a function of DNA lattice density. Dots: experimental data of Figure 17 in ref 5; solid curve is eq 17, dashed curve is B_0. Parameters: $D = 20$ Å, $1/\kappa = 60$ Å, $\theta = 0.9$.

electrostatic forces acting in DNA−CL complexes[59]

$$B = h^2(\partial^2 E_{el}/\partial h^2)_{h=h_{eq}} \tag{17}$$

and neglect other possible force contributions (van der Waals charge fluctuation forces,[33] the hydration DNA−DNA forces[33] caused by the ordering of water molecules, etc.; see ref 25 and section V of ref 5 where the influence of some of these forces on B has been considered in detail).

Using the energy expression in eq 13 and varying σ, we calculate h_{eq} and then $B(h_{eq})$ according to eq 17. We observe the $B(h)$ dependence with the slope of about −2 in the log−log plot, solid curve in Figure 7. The homogeneous term of eq 13 for $h_{eq} = h_{EN}$ (this works for $\kappa D \ll 1$) leads to the following estimate for B

$$B(h) \approx \frac{4\pi l_B k_B T}{D\kappa^2 b^2 h^2} \tag{18}$$

while the homogeneous term in a simpler energy expression eq 14 gives $B_0 \approx 2\pi l_B k_B T/(\kappa b^2 h^2)$. Smaller slab thicknesses D result in larger B values, while higher ionic strengths diminish B. Thus, in this approximation $B(h) \propto 1/h^2$, and it grows with the Debye screening length. So, we predict a power-law dependence for $B(h)$ rather than an exponential one. In Figure 7, we plot the results for $n_0 = 2.5$ mM that correspond to $1/\kappa \approx 60$ Å suggested as the ionic strength for the solution of DNA−CL complexes used in experiments. For this particular value of κ, the experimental data are best fitted with the DNA charge neutralization fraction of $\theta \approx 0.9$.

We take this value as a typical value of DNA charge neutralization. That is close to $\theta = 1 - 1/\xi \approx 0.76$ given by the counterion condensation theory for an isolated linear charge array in a low-salt electrolyte solution.[52] It is however not clear what will be the value of the charge neutralization fraction for a DNA rod confined between two oppositely charged lipid membranes that possess mobile charge groups.[61] This is an issue for a separate study. The value of 0.9 (as well as of 0.76) appears to be inconsistent with the experimental observation[2] that DNA is in the fully charged state in complexes with CL membranes, Figure 5. This fact might indicate the failure of the linearized PB approximation used here. It is however also possible that ion concentrations inside the complexes differ from their values in the bulk solution, which would change the best value of θ; see next subsection.

Let us discuss here some theoretical estimations for $B(h)$ available in the literature. In ref 5, for instance, on the basis of a simplified electrostatic calculation, no salt in solution and no low-dielectric membranes, the limit $B(h) \approx k_B T\pi l_B/(6b^2 h)$ has been suggested. In ref 21, the repulsive forces acting between DNA rods squeezed in salt-free between low-dielectric membranes have been calculated. In the limit of large DNA−DNA separations ($h \gg D$), the results were shown to give $B(h) \approx k_B T\pi D/(l_B h^2)$. These two results have different dependences on DNA−DNA separation h and have no κ-dependence at all. In ref 5, it was also shown that exponentially screened DNA−DNA hydration forces (with a decay length of ∼3 Å) as well as electrostatic screened rod−rod repulsion (with a Debye screening length of ∼60 Å, obtained for the ionic strength of the bulk solution used in experiments) are inconsistent with the experimental $B(h)$ data.

The small amount of available experimental data points as well as relatively large error bars (not shown in Figure 7) do not allow us however to decide which of the h-dependencies fits the experimental data better. Possible future experimental measurements of $B(h)$ at different salt concentrations in solutions can clarify also the point about $B(\kappa)$ dependence, supporting or falsifying the prediction of eq 18.

3.4. Donnan Equilibrium. Experimental measurements of B in DNA−CL lamellar complexes have been done in low-salt conditions.[5] However, the average salt concentration in the aqueous phase inside the DNA−CL complexes can differ from this bulk value due to the Donnan equilibrium, provided there is a mismatch of net charge densities of DNA lattice (σ_0) and of the lipid membranes (2σ). Then, for lamellar complexes of Figure 1b, the average reciprocal screening length is renormalized as follows

$$\tilde{\kappa}_L \approx \kappa\left[1 + \left(\frac{\sigma_0 + 2\sigma}{2n_0 e_0 D}\right)^2\right]^{1/4} \tag{19}$$

This expression can be modified to include a finite DNA diameter; i.e., in excess of DNAs over the CLs in the complexes, cations from solution will accumulate in the water phase inside the complexes due to on average negative potential there to preserve the electroneutrality. In addition to the Donnan effect, the variations of electrostatic potential in spaces between DNA rods make the screening length a position-dependent function, further modifying the DNA−DNA electrostatic interactions. Similarly, for the inverted hexagonal phase in the cylindrical cell model (Figure 1a) the value of the average inverse screening length is

$$\tilde{\kappa}_H \approx \kappa\left[1 + \left(\frac{1 - b/b_0}{2\pi b n_0 (R^2 - a^2)}\right)^2\right]^{1/4} \tag{20}$$

So, to use the correct value of κ for fitting the experimental data on $B(h)$, one needs also to know how far from electroneutrality were the actual complexes on which the $B(h)$ measurements have been performed.

4. Electrostatic Interactions in the Presence of Membranes

4.1. Interactions along a Salty Interface. Charged lipids confined to biological membranes are often quite mobile, and they can thus contribute to screening of DNA−DNA electrostatic interactions in DNA−CL lamellar complexes. The charges confined to a 2D membrane are known to obey the theory of 2D electrolyte solution developed, in particular, in refs 63−65. Let us consider one limit of this theory, when the interfacial screening with the inverse screening length $\kappa_s = 4\pi l_B n_s$ dominates over the bulk screening, $\kappa_s \gg \kappa$. (The concentration of mobile ions at the interface is n_s.) Then, at large distances

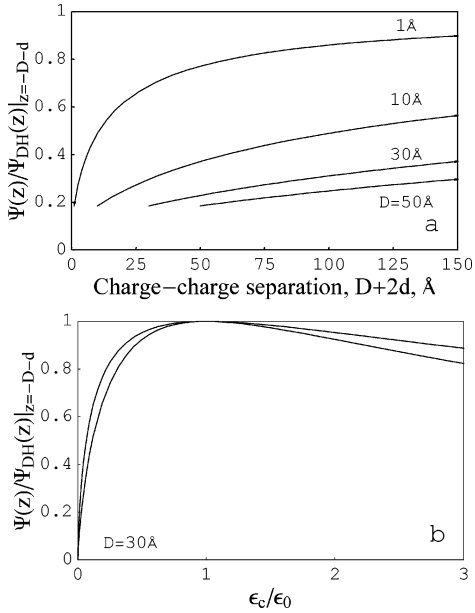

Figure 8. Electrostatic potential of a point unit charge, eq 24, in the salt-free limit ($\kappa = 0$, $r = 0$) on the opposite side of slabs with different thickness D as a function (a) of separation between the charges at $\epsilon_c/\epsilon_0 = 2/80$, and (b) of dielectric constants ratio at $D = 30$ Å for $d = 0$ (lower curve) and $d = 30$ Å (upper curve).

along such a salty interface ($\kappa_s r \gg 1$) the electrostatic potential of a charge positioned close to it becomes algebraically rather than exponentially screened. Namely, for a charge right on the interface (ϵ_c is the dielectric constant in space below the interface and ϵ is the dielectric constant in the aqueous medium above it) the potential is (eq 31 in ref 63 and eq 29 in ref 64)

$$\Psi(r) \approx \frac{l_B}{\left(1 + \frac{\epsilon - \epsilon_c}{\epsilon + \epsilon_c}\right)\kappa_s^2 r^3} \tag{21}$$

Then, the interaction energy of two strings of charges separated by the distance R along the interface can be obtained via summation of potentials from individual charges (per unit length)

$$\frac{E_{int}(R)}{k_B T} \approx \frac{2l_B}{\left(1 + \frac{\epsilon - \epsilon_c}{\epsilon + \epsilon_c}\right)b^2\kappa_s^2 R^2} \tag{22}$$

where b is the distance between the nearest charges along the string; see also eq 16 in ref 67.

4.2. Interactions across a Membrane. We calculate in this section the electrostatic potential created by a point unit charge positioned at the distance $z = d$ from the low-dielectric membrane, Figure 1d, which is modeled as an uncharged slab with dielectric constant ϵ_c with no mobile ions $\kappa_c = 0$. We solve the Laplace equation inside and the linear PB outside the membrane using the Fourier transformation in the membrane plane (x,y), $\Psi(x,y,z) = \int dk_x \int dk_y\, e^{ik_x x} e^{ik_y y} \tilde{\Psi}(k,z)$. Common conditions for Ψ and $d\Psi/dz$ at the dielectric boundaries and the condition $d\tilde{\Psi}(k, z)/dz|_{z=d\pm 0} = -l_B/\pi$ at the point of charge location are used. We obtain for the Fourier components of the potential on the opposite side of the membrane $\tilde{\Psi}$ (at $z < -D$), between the charge and the membrane $\tilde{\Psi}_{01}$ ($0 < z < d$),and at the same side of the membrane $\tilde{\Psi}_{02}$ at $z > d$ (Figure 1d)

$$\tilde{\Psi}(k,z) = \frac{2l_B\epsilon_0\epsilon_c k\, e^{-k_0 d}\, e^{(k_0+k)D}\, e^{k_0 z}}{\pi S}$$

$$\tilde{\Psi}_{01}(k, z) = \frac{l_B\, e^{-k_0 d}}{2\pi k_0}\left[e^{k_0 z} + \frac{e^{-k_0 z}(e^{2kD} - 1)(\epsilon_0^2 k_0^2 - \epsilon_c^2 k^2)}{S}\right] \tag{23}$$

$$\tilde{\Psi}_{02}(k, z) = \frac{l_B\, e^{-k_0 d}\, e^{-k_0 z}[\epsilon_0^2 k_0^2 (e^{2k_0 d} + 1)(e^{2kD} - 1) + 2\epsilon_0 k_0 \epsilon_c k (e^{2kD} + 1)\, e^{2k_0 d} + \epsilon_c^2 k^2 (e^{2k_0 d} - 1)(e^{2kD} - 1)]}{2\pi k_0 S}$$

Here $S \equiv (\epsilon_0 k_0 + \epsilon_c k)^2\, e^{2kD} - (\epsilon_0 k_0 - \epsilon_c k)^2$, $k^2 = k_x^2 + k_y^2$, $k_0^2 = k^2 + \kappa^2$, $r = \sqrt{x^2+y^2}$ is the distance from the charge along the membrane, and $J_0(kr)$ is the Bessel function of zeroth order. The corresponding potentials are

$$\Psi(r,z) = \int_0^\infty dk\, 2\pi k J_0(kr)\tilde{\Psi}(k,z) \tag{24}$$

As the membrane thickness diverges, $D \to \infty$, the $\tilde{\Psi}_{02}$ turns into the solution near a low-dielectric half-space

$$\tilde{\Psi}_{02}(k,z) \to \frac{l_B\, e^{-k_0 z}}{2\pi k_0}\left[\frac{\epsilon_0 k_0 - \epsilon_c k}{\epsilon_0 k_0 + \epsilon_c k}\, e^{-k_0 d} + e^{k_0 d}\right] \tag{25}$$

The electrostatic interactions are enhanced close to the interface (the first term in square brackets of eq 25 is the correction due to the boundary); see refs 64, 68, and 69. One limit of this expression is the potential of a charge positioned right at a low-dielectric ($\epsilon_c/\epsilon_0 \ll 1$) interface: Along this interface ($d = z = 0$) it appears to be twice as large as the Debye−Hückel potential in electrolyte solution

$$\Psi_{DH}(r) = l_B\, e^{-\kappa\sqrt{r^2+\Delta z^2}}/\sqrt{r^2 + \Delta z^2} \tag{26}$$

On the other side of the membrane, in the salt-free limit and at $r = 0$ the potential can be obtained analytically from eq 24; see also ref 70.

In general, the electrostatic interactions across the membrane are decreased due to the low-dielectric membrane interior (as compared to the $\epsilon_c = \epsilon$ and $\kappa_c = 0$ cases)—the lines of the electric field avoid passing through a low-dielectric medium. Figure 8 shows the ratio of $\Psi(r,z)$ in eq 23 to the Debye−Hückel potential. The dependence $\Psi(r)$ for different values of the screening parameters and dielectric constants, as obtained via numerical integration in eq 24, is plotted in Figure 9. The calculated dimensionless potential represents the electrostatic interaction energy (in units of $k_B T$) of the considered charge with an identical unit charge symmetrically positioned on the opposite side of the membrane.

4.3. Interaction of Charges in Solution between the Membranes. Let us also analyze shortly the solution for the potential created by a charge (positioned at $z = -D/2$) in electrolyte solution squeezed between two uncharged membranes with no mobile ions ($\kappa_c = 0$). The membranes are modeled as low-dielectric half-spaces positioned at $z > 0$ and $z < -D$; coordinates x and y are in the membrane plane. Then,

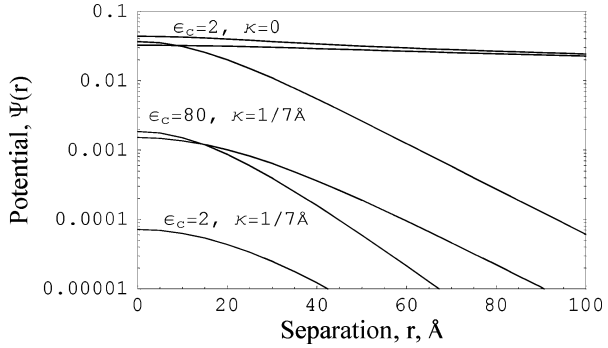

Figure 9. Electrostatic potential on the opposite side of the membrane as a function of r for different κ and ϵ_c values. (Two curves in each set correspond to $d = 0$ (top) and $d = 10$ Å (bottom curve), calculated for $D = 30$ Å.)

for the electrostatic potential in the aqueous medium at $-D < z < -D/2$ one can obtain

$$\Psi(r,z) = \int_0^\infty \mathrm{d}k\, 2\pi k J_0(kr) \times \frac{l_B\, \mathrm{e}^{-k_0 D/2}}{2\pi k_0} \frac{(\epsilon_c k + e_0 k_0)\, \mathrm{e}^{2k_0 D}\, \mathrm{e}^{k_0 z} + (\epsilon_0 k_0 - \epsilon_c k)\, \mathrm{e}^{-k_0 z}}{\epsilon_c k(\mathrm{e}^{k_0 D} + 1) + \epsilon_0 k_0(\mathrm{e}^{k_0 D} - 1)} \quad (27)$$

where $k_0 = \sqrt{k^2+\kappa^2}$. As one could expect, at small distances from the charge the potential is close to the Debye−Hückel result, eq 26. At large distances r however exponential $\mathrm{e}^{-\kappa r}/r$ screening turns into a power-law $1/r^3$ screening. The critical distance r at which this transition takes place grows as the separation between membranes D increases, Figure 10. The reason for this is that the electrolyte solution being squeezed between the membranes acts like a 2D electrolyte, where the same power-law screening is obtained; see ref 63 and eq 21 above.

4.4. Interaction of Two Arrays of Strings across the Membrane. In this section, we find the electrostatic energy for the system of two ordered arrays of infinitely thin charged strings interacting through a low-dielectric membrane, Figure 1c. The upper layer is longitudinally shifted with respect to the lower layer by the distance s. These arrays (supposed to mimic DNA layers in the lamellar phase) are assumed to be positioned right at the dielectric boundary (at $z = 0$ and $z = D$) and have the net charge density $\sigma_0 = -e_0/(bh)$. The possibility of membrane elastic deformations and screening by possibly mobile membrane lipids are neglected here.

We solve the linear PB equation both in aqueous (with dielectric constant ϵ and inverse screening length κ) and in the low-dielectric phase (ϵ_c and κ_c, $\kappa_c \neq 0$ for generality). We obtain for the Fourier components (eq 7) of the potential in aqueous medium at $z > D$, $\tilde{\varphi}_n(z) = (4\pi\sigma_0/\epsilon\kappa_n\Sigma_n)\, \mathrm{e}^{\kappa_n(D-z)}\{(1+\eta_n)[1 + \mathrm{e}^{\kappa_n cD}\mathrm{e}^{ings}] - (1-\eta_n)[1 + \mathrm{e}^{-\kappa_n cD}\mathrm{e}^{ings}]\}$. Here $\Sigma_n \equiv \mathrm{e}^{\kappa_n cD}(1+\eta_n)^2 - \mathrm{e}^{-\kappa_n cD}(1-\eta_n)^2$ and $\eta_n = \epsilon_c{}^{\kappa_n c}/(\epsilon\kappa_n)$; $\kappa_n^c = \sqrt{\kappa_c{}^2 + n^2 g^2}$, and $\kappa_n = \sqrt{\kappa^2 + n^2 g^2}$; $g = 2\pi/h$. Then, according to eq 12, we calculate the electrostatic energy $E_{el}(D)$ and interaction energy as

$$E_{int}(D,s) = E_{el}(D,s) - E_{el}(\infty) = \sum_{n=-\infty}^{\infty} \frac{8\pi\sigma_0{}^2\eta_n}{\epsilon\kappa_n\Sigma_n}\left[\cos(ngs) - \frac{1-\eta_n}{1+\eta_n}\mathrm{e}^{-\kappa_n cD}\right] \quad (28)$$

The $n = 0$ term of eq 28 describes the electrostatic interaction of planes with the homogeneously smeared charges, while the sum describes the energy variation upon a relative shift of the

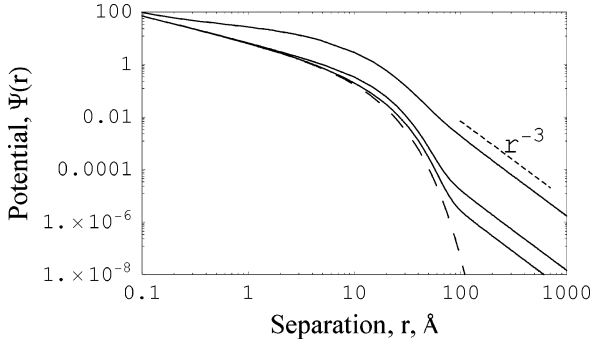

Figure 10. Potential of a point charge (eq 27) in the middle between two low-dielectric half-spaces separated by distance $D = 1$, 10, and 20 Å (solid curves from top to bottom) at $\kappa^{-1} = 7$ Å, $\epsilon_c/\epsilon_0 = 2/80$. The dashed curve is $\Psi_{DH}(r)$ in eq 26.

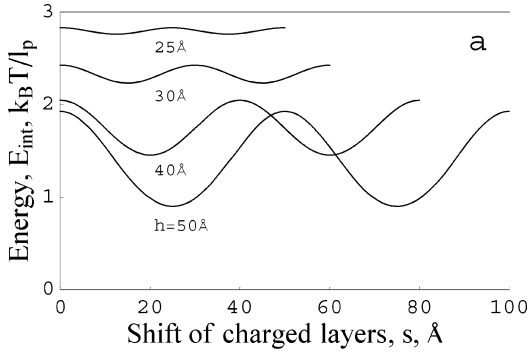

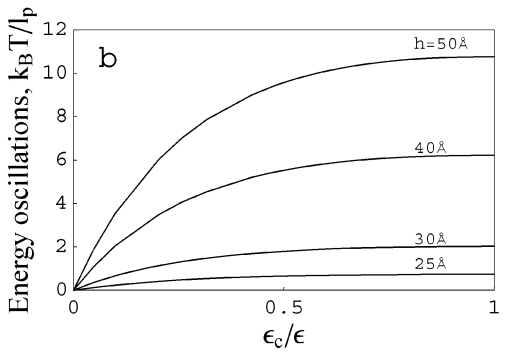

Figure 11. (a) Dependence of el interaction energy on mutual shift of charge layers for different h at $\epsilon_c/\epsilon = 2/80$. Two periods of oscillations are shown. (b) Magnitude of the energy oscillations as a function of ϵ_c/ϵ_0. Parameters: $\kappa = \kappa_c = 1/(7$ Å), $D = 30$ Å, $b = 1.7$ Å.

charge lattices. Typically, the $n = \pm 1$ terms in the sum, which describe the interaction of charge harmonics with the periodicity h, provide the main contribution to the energy oscillations. (Further terms in the sum rapidly decay with n.) For a uniform medium, with no dielectric slab and homogeneous electrolyte concentration ($\kappa_c = \kappa$ and $\epsilon_c = \epsilon$ everywhere; $\eta_n = 1$), one can obtain from eq 28 $E_{int}(D,s) = \sum_{n=-\infty}^{\infty} 2\pi\sigma_0{}^2\, \mathrm{e}^{-\kappa_n D}\cos(ngs)/(\epsilon\kappa_n)$.

We obtain that a low-dielectric slab impedes the electrostatic interactions, resulting in reduction of the interaction energy oscillations, Figure 11b. (We used here $\kappa_c = \kappa$, i.e., $\eta_n = \epsilon_c/\epsilon$.) Also, the E_{int} oscillations become more pronounced for larger string−string separations h, Figure 11a. In this figure, the interaction energy being averaged over $E_{int}(s)$ oscillations scales as $\propto \sigma_0{}^2$ and decreases with increases of h because $\sigma_0 \propto 1/h$. Energy oscillations decay with the thickness of the low-dielectric layer D; they grow with decreases of κ_c and κ. Magnitudes of oscillations in low-salt solutions and for thin membranes can reach several k_BT per DNA persistence length $l_p \approx 500$ Å for the typical values of parameters.

5. Two-Dimensional DNA Condensation and Interaction of DNA Helices

In this section, we discuss some aspects of DNA charge helicity of DNA−DNA intermolecular interaction in DNA−CL complexes in the presence of multivalent cations. We work in this section on the same level of the linear PB equation, but the double-stranded DNA is considered now as two paired helical spirals of charges rather than as a featureless uniformly charged rod. We do not solve here the problem of interactions of helical-like DNAs in DNA−CL lamellar and inverted hexagonal complexes, in the presence of confinement of electrolyte solution, dielectric boundaries, and mobile membrane surface charges. This is a separate complicated problem. We use here the results of a recently developed theory of DNA−DNA interaction in electrolyte solution. We point out here that DNA−DNA separations in 2D condensed DNA−CL lamellar complexes with di- and trivalent DNA-condensing cations ($h \approx 28$ Å)[9] are very close to those in 3D hexagonal DNA condensates.[33,72] To our knowledge, the electrostatics of 2D DNA condensation in lamellar complexes with polyvalent cations has not yet been studied theoretically.

5.1. Electrostatic Interaction of DNA Duplexes. Let us start with the theory of electrostatic interactions of DNA double helices.[34−38] The main concept of this theory is that the helical charge patterns on DNAs give rise to a zipper-like DNA−DNA electrostatic attraction for intermediate DNA−DNA separations, $h \approx 25-35$ Å, for the typical DNA parameters in the model. The theory thus predicts the attraction between net likely charged helices without invocation to correlations in the profiles of counterions condensed near the DNA surface. The decay length of this attraction is shorter than the Debye length of $1/\kappa$ for repulsion of homogeneously charged objects. The DNA helicity is treated explicitly in this theory (both the positions of DNA phosphates and of cations adsorbed on DNA) together with the Debye−Hückel screening of charges and the low-dielectric DNA molecular core. For short separations between DNAs, at $h \lesssim 24$ Å, the theory predicts an electrostatic fast-decaying repulsion originating from the repulsion of charges on one DNA and image charges induced in the core of another DNA. At large h, when the attraction due to DNA charge helicity is already screened, the nearly exponentially decaying repulsion of homogeneously charged DNA rods is recovered.[71] Being caused by separation of positive and negative charges along the DNA axis, this zipper-like attraction is most pronounced for well-neutralized DNAs (high charge compensation fractions, θ is close to 1) and for preferential adsorption of cations in DNA major groove. The expression for DNA−DNA interaction energy $E_{int}(h,f,\theta)$ is quite cumbersome, and it is provided in the original papers (see eq 12 in ref 35, eqs A1−A7 in ref 38, and eqs A1 and A2 in ref 43). In what follows below, only the first three terms of the exact solution for $E_{int}(R)$ are taken into account, which give the dominant contributions in the region of parameters considered.

There exist of course a number of other/different models and theories that describe attraction between likely charged cylindrical molecules mimicking the DNA−DNA attraction and condensation.[73] The majority of them are based on the idea of correlated fluctuations in distributions of condensed multivalent counterions[74] on surfaces of two juxtaposed highly charged rods.[75] Sharing of condensed multi- and monovalent counterions has also been suggested as a possible DNA−DNA attraction mechanism.[76] Almost all of these models however neglect the helicity of the DNA charge distribution and the effects of the low-dielectric DNA core. The whole idea of properly aligned counterion charge density waves is based on the assumption that adsorbed ions are quite mobile on the DNA surface. This might however not be the case, especially for multivalent counterions known to bind strongly to DNA (both chemically and electrostatically). Also, the idea of 1D Wigner-crystal-like long-range counterion correlations along the DNA has not been proven explicitly for cylindrical geometry. Recent computer simulations,[77] for example, indicate that these correlations along DNA are rather short-ranged. Detailed molecular dynamics simulations (see discussion in ref 78) for different cations in the solution and for various DNA sequences, with correctly chosen potentials for ion−DNA and ion−ion interactions, have to be performed to elucidate the realistic degree of counterion association to DNA, cations partitioning on DNA surface, and cation mobility along DNA. There are several good reviews on the subject; we have also addressed some aspects of it in previous publications.

Our theory of DNA−DNA electrostatic interactions has of course also its limitations. (The linear Debye−Hückel rather than the nonlinear PB theory is used, ionic correlations in electrolyte solution are neglected, adsorbed cations are modeled as point-like charges or thin continuous charged spirals, a sharp dielectric contrast of DNA with electrolyte solution is assumed, some assumptions made about the counterion distribution on DNA affect dramatically the outcomes of the model, etc.). This theory has been modified to include specific base-pair nonideality of DNA structure and a finite torsional elasticity of the DNA backbone[38] as well as the effects of DNA base pair fluctuations at elevated temperatures.[39] The theory and its generalizations have been successfully applied to the description of a number of DNA-related phenomena, in particular, to rationalizing the decay lengths between charged biological helices,[34] the description of DNA−DNA forces in dense molecular assemblies,[37] DNA electrostatically induced structural transitions,[40,41] the mechanism of DNA−DNA electrostatic recognition,[36,38] DNA sequence-dependent and cation-specific condensation,[35,37] DNA torsional interaction-induced deformations,[38,44] azimuthal DNA frustrations in dense DNA columnar assemblies,[38,39] DNA melting in dense aggregates under osmotic stress,[43] the structure of DNA toroids,[42] as well as the structure of dense phases of nucleosome core particles.[45]

5.2. DNA−DNA Separations in 3D and 2D DNA Condensates. DNA−DNA forces are often studied in DNA precipitates and dense assemblies.[31,33] In particular, the dependence of equilibrium DNA−DNA separations h_{eq} in DNA−polyamine precipitates has recently been measured by X-ray diffraction.[72] Both 146-bp-long nucleosomal DNA fragments and 48.5-kbp-long λ-DNA have been used for condensation in the presence of spermine^{4+}, spermidine^{3+}, and cobalt hexammine^{3+}. For small DNA concentrations, <3 mM, the value of h_{eq} was shown to increase from ∼28.3 to 29.3 Å with the increase of spermine concentration from $n_{sp} = 1$ to 100 mM, whereas for DNA concentration of 90 mM a nonmonotonous behavior of $h_{eq}(n_{sp})$ has been detected, Figures 4 and 5 in ref 72. The redissolution of DNA precipitates has been observed at ∼120 mM of spermine. One could suggest that interhelical separations in DNA condensates increase upon approach of this condensation−redissolution boundary on the phase diagram. Equilibrium separations were shown to increase slightly with the addition of NaCl; also, higher n_{sp} values are required to induce DNA condensation at higher concentrations of simple salt n_0.

In Figure 12, left panel, we present the results for DNA−DNA separations h_{min} in the minimum of interaction energy E_{int} as obtained from the theory of refs 34, 35, and 37 for $\theta =$

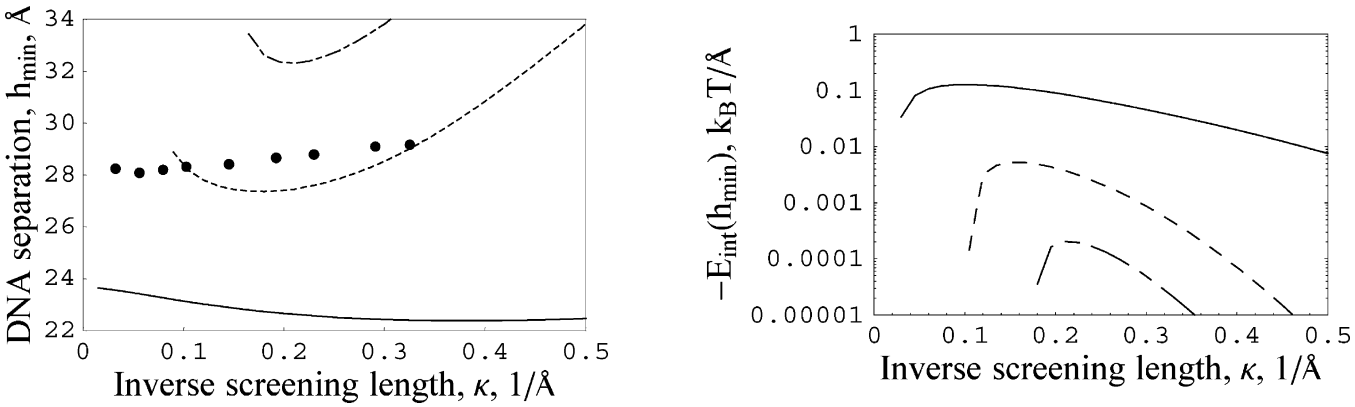

Figure 12. DNA−DNA separations h_{min} in the minimum of interaction energy E_{int} (left panel) as calculated from the theory of duplex−duplex interactions of refs 34, 35, and 37 at $\theta = 0.8$, $f = 0$ (solid), $f = 0.3$ (dotted), and $f = 1$ (dot−dashed curve). The dots are experimental interhelical separations in DNA precipitates with spermine^{4+}.[72] Right panel shows the DNA−DNA attraction strength, $E_{int}(h_{min})$.

0.8 and different partitioning of adsorbed cations f on DNA. (The fraction f of cations is adsorbed in the minor groove, and the $(1 - f)$ fraction is adsorbed in the major DNA groove.) Starting at this critical separation, the forces between DNAs, $F_{int} = -\partial E_{int}/\partial h$, become attractive and stay attractive up to some separation (not shown). The distribution of cations between DNA grooves has a considerable effect on h_{min} in the theory. The molecules with smaller f values (stronger cation adsorption into the DNA major groove) attract each other typically stronger. In Figure 12, we show also the data of ref 72 for $h_{eq}(n_{sp})$ for DNA precipitates with spermine. The experimental tendency of a weak increase of equilibrium separations with increase of salt concentration is qualitatively captured by the theory. In the model, the change in n_{sp} was supposed to affect only the value of κ in solution between DNAs but not the faction θ; that is a questionable assumption though. The choice of $f = 0.3$ gives the most close agreement to the experimental data for the chosen value of $\theta = 0.8$ (Spermine is indeed known to bind preferentially into the major DNA groove that results in small f values in the model.) Also, upon increase of θ toward unity, the separations between DNAs become smaller and the attraction strength grows (not shown).

The right panel of Figure 12 shows the calculated value of $E_{int}(h_{min})$, i.e., the maximal depth of DNA−DNA attraction energy. We observe that DNA molecules attract each other in a limited range of salt concentrations due to an interplay of different terms in the electrostatic interaction energy. Namely, in the limit of high salt the DNA−DNA zipper-like attraction is progressively shielded by electrolyte, while at low salt the repulsive contributions of image forces at small DNA−DNA distances and of uniformly charged rods at large distances suppress the intermolecular attraction at intermediate distances.

On the basis of the analysis of energetics of DNA aggregates, the cohesive DNA−DNA electrostatic energy of $\sim 0.015 k_BT$/Å has been suggested for separations $h_{eq} \approx 30$ Å in ref 72. We can obtain similar magnitudes of DNA−DNA forces from the theory, strongly dependent however on θ, f, and κ values used (see ref 37 where the magnitude of DNA−DNA electrostatic forces has been described in details and quantitatively compared with the pressure−distance curves obtained by the osmotic stress measurements on dense DNA assemblies[32,33]).

Two-dimensional DNA condensation with condensing cations inside DNA−CL lamellar complexes is likely to have some similarities with the described electrostatically driven DNA condensation in three dimensions. As the condensing salt is added into solution, multivalent cations replace Na^+ inside DNA−CL complexes and concentrate in the vicinity of DNAs. According to the cations' adsorption isotherm on DNA, this thus results in a larger amount of cations bound/adsorbed on the DNA. At some critical concentration of multivalent salts, the value of θ reaches the critical value at which DNAs start to attract each other in the theory. Similar attraction mechanisms might trigger 2D condensation in lamellar complexes and induce an abrupt drop of DNA−DNA separations down to ~28 Å.[9]

Three-dimensional DNA condensates are known to resolubilize upon addition of a large amount of multivalent salts[72] as the attraction between DNAs is weakened. Two possible reasons for this are: The DNAs become overneutralized by adsorbed cations or attractive interactions become progressively screened. Similarly, one can speculate that in condensed DNA−CL lamellar complexes at higher amounts of multivalent cations, DNA−DNA attraction may be weakened or even disappear. This would result in an increase of h_{eq} upon further addition of di- and trivalent cations. That can be checked in future experimental studies on the thermodynamics of DNA−CL assembly.

6. Conclusions and Outlook

We have calculated the electrostatic energy of DNA rods in lamellar and inverted hexagonal phases with cationic lipids. Adding the cost of elastic membrane deformations for the hexagonal phase, one could in principle study the phase behavior and stability of DNA−CL complexes as a function of the system parameters (water content, charge density of the lipid membrane, the ratio of rod and membrane charge densities, etc.). Analytical treatment of equilibrium adsorption of DNA onto lipid bilayers and onto DNA−CL complexes of different morphologies is however a complicated task,[18] which is beyond the scope of the present paper. Also, the different models used for the description of DNA charges in the lamellar and the inverted hexagonal phase in the present paper—uniformly charged cylinder vs thin charged string—are not expected to provide quantitatively reliable results, as compared to those obtained in ref 18 on the basis of the same model for both complex morphologies. We have also provided analytical solutions for some problems of charge−charge interactions in the presence of dielectric discontinuities, including two-dimensional electrolyte screening, interaction of charges across the membrane and charges squeezed between the membranes in solution. We have discussed the strength of positional correlation of neighboring DNA layers across the DNA−CL lamellar stack. We have also discussed how the helical charge motif of the DNA surface can regulate DNA−DNA separations in DNA layers condensed in two dimensions in lamellar complexes of DNA with cationic lipids.

As it was noted in the introduction, DNA−CL complexes are used as gene delivery vectors.[1] Together with two other popular techniques (viral vectors and transport of naked DNAs), the complexes are used nowadays mainly for medical treatments of different types of cancer. DNA−CL-based carriers can allow transfection of DNA fragments of up to 10^6 bp in length, comparably longer than typical viral-based carriers do, around 40 kbp DNA (being limited by the typical size of genomes of viruses used (some DNA-based adenoviruses and pox viruses and RNA-based retroviruses)). Another advantage of DNA−CL complexes is that such vectors do not trigger the immune response of cells, contrary to that caused by viral proteins. The main disadvantage of DNA−CL-based carriers is their comparably low transfection efficiency. The basic obstacles are the impeded translocation of complexes across cellular membranes and some problems with DNA release from the complexes inside the cells.

The release of DNA from complexes in vitro takes place upon addition of some multivalent counterions into solution. These cations "strip" DNA from lipid membranes and cause a 3D DNA condensation in solution.[1,9] In cells, DNA-condensing agents such as histone proteins or spermine cations are available in millimolar concentrations during the cell cycle and can also in principle be used for the release of DNA. The development of most effective DNA carriers in terms of complex size and morphology, DNA density, and lipid composition is the primarily goal of the nonviral gene therapy research.

The properties of supramolecular DNA−CL assembly and interactions inside the DNA−CL complexes as well as of the complexes with cellular membranes—the main determinants of complex functioning and stability—are however still far from being completely understood. For instance, positively charged DNA−CL complexes are typically used for transfection that facilitates the electrostatic attractions of complexes with the oppositely charged cell surface.[1] In general, inverted hexagonal DOPE-based DNA−CL complexes are transfected more efficiently than the lamellar complexes. Multivalent lipids MVL5 were shown to produce up to 3 orders of magnitude higher transfection efficiencies than monovalent DOTAP lipids.[1]

The charge density of the lipid membrane σ was shown to be the universal parameter that controls the transfection efficiency of lamellar DNA−CL complexes. The efficiency increases nearly exponentially with σ, suggesting the existence of a barrier to endosomal fusion.[1] Lamellar complexes with the lipid membrane at charge densities of $\sigma \approx e_0/200$ Å^2 were shown to stay intact within the cells, whereas the complexes with $\sigma \gtrsim e_0/120$ Å^2 release their DNAs in the form of aggregates.[1] (Spermine and histones were present in the transfected cells studied.) Transfection efficiency saturates at about $e_0/100$ Å^2 for both membranes with monovalent (DOTAP) and multivalent dimethylpropanaminiumtrifluoroacetate (DOSPA) lipids.[8] The barrier for entry of lamellar DNA−CL complexes into the cell contains two terms:[1] the energy cost of elastic deformations of the cellular membrane and the negative energy term due to favored adhesion of positively charged complexes to negatively charged cell/plasma membrane. The latter was shown to be responsible for a strong σ-dependence of the transfection efficiency.[1] Although it is easier to transmit the complexes with large σ values across a membrane, it might be more difficult to release the DNA from such complexes that will then limits their transfection efficiency.[1]

On the contrary, the membrane charge density has almost no effect on transfection efficiency of inverse hexagonal DNA−CL complexes.[1] Their translocation is governed by a different mechanism. Namely, although the lipids used for inverted hexagonal complexes possess a negative spontaneous curvature, the outer lipid layer covering the whole DNA−CL particle has a positive curvature (to provide a hydrophilic surface around the complex). This elastically unstable conformation of outer lipids drives a rapid fusion of complexes with cellular membranes. As a result, the outer DNA layer of the complex is released into the solution, and a smaller complex is formed.[1] This process is believed to be largely independent of σ.

The effect of electrostatic interactions (DNA−membrane, membrane−membrane, along the membrane, the membrane bending undulations[79]) as well as of membrane interfacial tension and bending rigidity[80] on the formation of membrane vesicles, on the fusion of DNA−CL complexes with cellular membranes, and on DNA release form the complexes might be interesting subjects for the future theoretical research.

Acknowledgment. I thank D. Harries for useful comments and for a critical reading of an earlier version of the manuscript. A part of this work was done after the submission of a proposal for the Emmy Noether DFG program.

References and Notes

(1) Ewert, K. K.; Ahmad, A.; Evans, H. M.; Safinya, C. R. *Expert Opin. Biol. Ther.* **2005**, *55*, 33.
(2) Raedler, J. O.; Koltover, I.; Salditt, T.; Safinya, C. R. *Science* **1997**, *275*, 810.
(3) Koltover, I.; Salditt, T.; Raedler, J. O.; Safinya, C. R. *Science* **1998**, *281*, 78.
(4) Salditt, R.; Koltover, I.; Raedler, J. O.; Safinya, C. R. *Phys. Rev. Lett.* **1997**, *79*, 2582.
(5) Salditt, T.; Koltover, I.; Raedler, J. O.; Safinya, C. R. *Phys. Rev. E* **1998**, *58*, 889.
(6) Artzner, F.; Zantl, R.; Rapp, G.; Raedler, J. O. *Phys. Rev. Lett.* **1998**, *81*, 5015.
(7) Wagner, K.; Harries, D.; May, S.; Kahl, V.; Rädler, J. O.; Ben-Shaul, A. *Langmuir* **2000**, *16*, 303.
(8) Lin, A. J.; Slack, N. L.; Ahmad, A.; George, C. X.; Samuel, C. E.; Safinya, C. R. *Biophys J.* **2003**, *84*, 3307.
(9) Koltover, I.; Wagner, K.; Safinya, C. R. *Proc. Natl. Acad. Sci. U.S.A.* **2000**, *97*, 14046.
(10) Liang, H.; Harries, D.; Wong, G. C. *Proc. Natl. Acad. Sci. U.S.A.* **2005**, *102*, 11173.
(11) Koltover, I.; Salditt, T.; Safinya, C. R. *Biophys. J.* **1999**, *77*, 915.
(12) Yang, L.; Liang, H.; Angelini, T. E.; Butler, J.; Coridan, R.; Tang, J. X.; Wong, G. C. L. *Nat. Mater.* **2004**, *3*, 615.
(13) Raviv, U.; Needleman, D. J.; Li, Y.; Miller, H. P.; Wilson, L.; Safinya, C. R. *Proc. Natl. Acad. Sci. U.S.A.* **2005**, *102*, 11167.
(14) Gelbart, W. M.; Bruinsma, R. F.; Pincus, P. A.; Parsegian, V. A. *Phys. Today* **2000**, *53*, 38 and references therein.
(15) Bruinsma, R. *Eur. Phys. J. E* **1998**, *4*, 75.
(16) Caracciolo, G.; Pozzi, D.; Amenitsch, H.; Caminiti, R. *ChemPhysChem* **2006**, *429*, 250.
(17) Harries, D.; May, S.; Gelbart, W. M.; Ben-Shaul, A. *Biophys. J.* **1998**, *75*, 159.
(18) May, S.; Harries, D.; Ben-Shaul, A. *Biophys. J.* **2000**, *78*, 1681.
(19) Harries, D.; May, S.; Ben-Shaul, A. *J. Phys. Chem. B* **2003**, *107*, 3624.
(20) Podgornik, R.; Harries, D.; Parsegian, V. A.; Strey, H. H. In *Molecular Interaction in Lipids, DNA, and DNA−Lipid Complexes in Gene Therapy−Therapeutic Mechanisms and Strategies*, 2nd ed.; Templeton, N. S., Ed.; 2004.
(21) Bruinsma, R.; Mashl, J. *Europhys. Lett.* **1998**, *41*, 165.
(22) Caracciolo, G.; Caminiti, R. *Chem. Phys. Lett.* **2004**, *400*, 314.
(23) Farago, O.; Gronbech-Jensen, N.; Pincus, P. *Phys. Rev. Lett.* **2006**, *96*, 018102.
(24) Farago, O.; Cronbech-Jensen, N. *Biophys. J.* **2007**, *92*, 3228.
(25) Gonzalez-Amercua, O.; Hernandez-Contreras, M. *J. Chem. Phys.* **2005**, *123*, 224906.
(26) O'Hern, C. S.; Lubensky, T. C. *Phys. Rev. Lett.* **1998**, *80*, 4345.
(27) Dan, N. *Biophys. J.* **1996**, *71*, 1267.
(28) Schiessel, H.; Aranda-Espinoza, H. *Eur. Phys. J. E* **2001**, *5*, 499.
(29) Wagner, A. J.; May, S. *Electrostatic interactions across a charged lipid bilayer*; http://arxiv.org/pdf/cond-mat/0607733.
(30) In ref 27, for instance, it was suggested that upon DNA adsorption on a lipid membrane the packaging of lipids is perturbed, giving rise to attractive undulation-induced interactions between DNA rods competing with direct electrostatic rod−rod repulsion. In ref 28, the effect of rod−rod and membrane−membrane repulsive and rod−membrane attractive

electrostatic interactions in a DNA−CL lamellar stack on the membrane conformational properties has been considered. It was suggested that rod−membrane attraction favors a compression of the stack in a direction perpendicular to the membrane: The undulations of neighboring membranes are phased so that they produce a better embracing of intercalated oppositely charged DNA rods. It was shown that isoelectric complexes are favored in the weak screening regime, while DNA negatively overcharged complexes minimize the electrostatic energy in the strong screening limit, when the screening length is much smaller than the separation between the membranes. The amplitude of the membrane undulations was estimated to be ∼1 Å in the weak screening regime for typical DNA−CL complex parameters. Note that no dielectric contrast and no lipid demixing have been considered in this electrostatic model. Recently, the problem of rod−rod interaction across a low-dielectric membrane has been considered within the nonlinear PB theory in ref 29. The authors have argued that as large electric fields originating from the rods do not efficiently penetrate the lipid membrane the electrostatic coupling of the rods is diminished. Considerable coupling of two rods on opposite sides of the membrane, $\sim 10k_BT$ per DNA persistence length l_p, has been predicted in the limit of low salt and thin membranes.[29] The mobility of lipids on the membrane surface was shown to result in a reduction of rod−rod electrostatic coupling across the membrane.

(31) Bloomfield, V. A. *Biopolymers* **1991**, *31*, 1471.

(32) Rau, D. C.; Parsegian, V. A. *Biophys. J.* **1992**, *61*, 260.

(33) Leikin, S.; Parsegian, V. A.; Rau, D. C.; Rand, R. P. *Annu. Rev. Phys. Chem.* **1993**, *44*, 369.

(34) (a) Kornyshev, A. A.; Leikin, S. *J. Chem. Phys.* **1997**, *107*, 3656. (b) Kornyshev, A. A.; Leikin, S. *J. Chem. Phys.* **1998**, *108*, 7035(E).

(35) Kornyshev, A. A.; Leikin, S. *Phys. Rev. Lett.* **1999**, *82*, 4138.

(36) Kornyshev, A. A.; Leikin, S. *Phys. Rev. Lett.* **2001**, *86*, 3666.

(37) Cherstvy, A. G.; Kornyshev, A. A.; Leikin, S. *J. Phys. Chem. B* **2002**, *106*, 13362.

(38) Cherstvy, A. G.; Kornyshev, A. A.; Leikin, S. *J. Phys. Chem. B* **2004,** *108*, 6508.

(39) Lee, D. J.; Wynveen, A.; Kornyshev, A. A. *Phys. Rev. E* **2004**, *70*, 051913.

(40) Kornyshev, A. A.; Leikin, S. *Proc. Natl. Acad. Sci. U.S.A.* **1998**, *95*, 13579.

(41) Cherstvy, A. G. *J. Chem. Phys.* **2005**, *123*, 116101.

(42) Cherstvy, A. G. *J. Phys.: Condens. Matter* **2005**, *17*, 1363.

(43) Cherstvy, A. G.; Kornyshev, A. A. *J. Phys. Chem. B* **2005**, *109*, 13024.

(44) Kornyshev, A. A.; Lee, D. J.; Leikin, S.; Wynveen, A.; Zimmerman, S. B. *Phys. Rev. Lett.* **2005**, *95*, 148102.

(45) Cherstvy A. G.; Everaers, R. *J. Phys.: Condens. Matter* **2006**, *18*, 11429.

(46) On the contrary, for the hexagonal assembly of charged rods in electrolyte solution the electrostatic potential $\Psi(r) = [2\xi/\kappa a][I_1(\kappa R_s)K_0(\kappa r) + K_1(\kappa R_s)I_0(\kappa r)]/[I_1(\kappa a)K_1(\kappa R_s) - K_1(\kappa a)I_1(\kappa R_s)]$ becomes more negative than $\Psi_0(r)$ with compression of assembly, which results in nearly exponential growth of the rod energy in assembly; see ref 37.

(47) Cherstvy, A. G.; Winkler, R. G. *J. Chem. Phys.* **2004**, *120*, 9394.

(48) Cherstvy, A. G.; Winkler, R. G. *Phys. Rev. Lett.* **2006**, *96*, 066103.

(49) Cherstvy, A. G.; Winkler, R. G. *J. Chem. Phys.* **2006**, *125*, 064904.

(50) Poghossian, A.; Cherstvy, A.; Ingebrandt, S.; Offenhäusser, A.; Schöning, M. J. *Sens. Actuators, B* **2005**, *111*−*112*, 470.

(51) Cherstvy, A. G. *J. Phys. Chem. B* **2006**, *110*, 14503.

(52) (a) Manning, G. S. *Q. Rev. Biophys.* **1978**, *11*, 179. (b) Manning, G. S. *J. Chem. Phys.* **1969**, *51*, 924. (c) Manning, G. S. *J. Chem. Phys.* **1969**, *51*, 934. (d) Manning, G. S. *J. Chem. Phys.* **1969**, *51*, 3249.

(53) Baumann, C. G.; Smith, S. B.; Bloomfield, V. A.; Bustamante, C. *Proc. Natl. Acad. Sci. U.S.A.* **1997**, *94*, 6185.

(54) Note that the DNA persistence length is strongly dependent on the concentration and the valence of counterions in electrolyte solution. The dependence of l_p on n_0[53] appears to be consistent with the Odijk−Skolnick−Fixman theory of the polyelectrolyte electrostatic persistence[55] with the DNA linear charge density renormalized due to the counterion condensation[52] down to one charge per l_B along the DNA axis (see however the discussion in ref 56 on this subject). The persistence length reaches the limiting value of ∼500 Å at high salt concentrations (≳0.01−0.1 M), and it increases to 1000 Å at about 0.001 M NaCl.[53] At 5−25 μM concentrations of multivalent DNA-condensing cations, such as cohexammine^{3+} and spermidine^{3+}, the l_p of DNA descreses 2−3 times as compared to its value in monovalent salt solutions. In the main text, the canonical value of $l_p \approx 50$ nm at physiological conditions is used. Note also that upon DNA adsorption on positevely charged surfaces DNA persistence length can be significantly (as much as 5-fold) reduced; see ref 57. For spermidine^{3+} or poly-L-ornithine coated mica surfaces, the DNA persistence length was shown to decrease as a function of the surface charge density. This l_p decrease has been attributed to the assymetric charge neutralization caused by the binding of these cations to DNA;[56] see also ref 58. This effect might also be relavant to DNA confinement between positively charged membranes in DNA−CL complexes. This is however a subject for a separate investigation.

(55) (a) Skolnick, J.; Fixman, M. *Macromolecules* **1977**, *10*, 944. (b) Odijk, T. J. *J. Polym. Sci.* **1977**, *15*, 477.

(56) Manning, G. S. *Biophys. J.* **2006**, *91*, 3607.

(57) Podesta, A.; Indrieri, M.; Brogioli, D.; Manning, G. S.; Milani, P.; Guerra, R.; Finzi, L.; Dunlap, D. *Biophys. J.* **2005**, *89*, 2558.

(58) Strauss, J. K.; Maher, L. J., III. *Science* **1994**, *266*, 1829.

(59) Note that the compressibility modulus of the lipid membrane itself was roughly estimated in ref 5 as $2k_BT/Å^2$, independently on the value of *h*, which is a questionable assumption. Also, the values of *B* measured in experiments are considerably smaller than this estimate. The value of the lipid membrane compression measured for a membrane stack is $\sim 5 \times 10^{-5} k_BT/Å^3$.[60]

(60) Richetti, P.; Kékicheff, P.; Parker, J. L.; Ninham, B. W. *Nature* **1990**, *346*, 252.

(61) The degree of counterion released form a DNA rod adsorbed in the vicinity of an oppositely charged planar surface has been studied in low-salt limit in ref 62. It has been shown in particular that if the surface Gouy−Champan length is much larger than the rod radius (weakly charged surfaces), most of the condensed cations still stay near the rod. However, when the charges on the surface are allowed to move freely, almost complete release of condensed counterions from the rod has been predicted for situations when the Gouy−Champan length is of the order of the rod radius.

(62) Sens, P.; Joanny, J.-F. *Phys. Rev. Lett.* **2000**, *84*, 4862.

(63) Muller, V. M.; Derjaguin, B. V. *J. Colloid Interface Sci.* **1977**, *61*, 361.

(64) Netz, R. R. *Phys. Rev. E* **1999**, *60*, 3174.

(65) In ref 66 the interaction between a uniformly charged rod and a fluid membrane with a charge density that depends on the pH level has been considered. The PB boundary value problem has been solved with the charge-regulation boundary conditions modified due to the mobility of lipids on the membrane. It was obtained in particular that, due to redistribution of mobile charges of both signs on the membrane, at small rod−membrane separations their electrostatic interaction energy decreases considerably. The energy can become even attractive for a negatively charged rod in front of on average negatively charged membrane due to a positively charged patch on the membrane underneath the DNA rod.

(66) Fleck, C.; Netz, R. R.; von Gruenberg, H. H. *Biophys. J.* **2002**, *82*, 76.

(67) Menes, R.; Gronbech-Jensen, N.; Pincus, P. A. *Eur. Phys. J. E* **2000**, *1*, 345.

(68) Stillinger, F. H., Jr. *J. Chem. Phys.* **1961**, *35*, 1584.

(69) Allen, R. J.; Hansen, J. P.; Melchionna, S. *Phys. Chem. Chem. Phys.* **2001**, *3*, 4177.

(70) Netz, R. R. *Eur. Phys. J. E* **2000**, *3*, 131.

(71) Brenner, S. L.; Parsegian, A. V. *Biophys. J.* **1974**, *14*, 327.

(72) Raspaud, E.; Durand, D.; Livolant, F. *Biophys. J.* **2005**, *88*, 392 and references therein.

(73) (a) Rouzina, I.; Bloomfield, V. A. *J. Phys. Chem.* **1996**, *100*, 9977. (b) Gronbech-Jensen, N.; Mashl, R. J.; Bruinsma, R. F.; Gelbart, W. M. *Phys. Rev. Lett.* **1997**, *78*, 2477. (c) Ha, B.-J.; Liu, A. J. *Phys. Rev. Lett.* **1997**, *79*, 1289. (d) Barrat, J. L.; Joanny, J. F. *Adv. Chem. Phys.* **1996**, *94*, 1. (e) Shklovskii, B. I. *Phys. Rev. Lett.* **1999**, *82*, 3268. (f) Grosberg, Yu. A.; Nguyen, T. T.; Shklovskii, B. I. *Rev. Mod. Phys.* **2002**, *74*, 329. (g) Allahyarov, E.; Gompper, G.; Löwen, H. *Phys. Rev. E* **2004**, *69*, 041904. (h) Lau, A. W.; Pincus, P.; Levine, D.; Fertig, H. A. *Phys. Rev. E* **2001**, *63*, 051604. (i) Levin, Y. *Rep. Prog. Phys.* **2002**, *65*, 1577. (j) Boroudjerdi, H.; Kim, Y.-W.; Naji, A.; Netz, R. R.; Schlagberger, X.; Serr, A. *Phys. Rep.* **2005**, *416*, 129. (k) see also the discussion in Kornyshev, A. A.; Lee, D. J.; Leikin, S.; Wynveen, A. *Rev. Mod. Phys.*, in press.

(74) (a) Kjellander, R.; Marčelja, S. *Chem. Phys. Lett.* **1986**, *127*, 402. (b) Kirkwood, J. G.; Schumaker, J. B. *Proc. Natl. Acd. Sci. U.S.A.* **1952**, *38*, 863.

(75) (a) Oosawa, F. *Biopolymers* **1968**, *6*, 134. (b) Oosawa, F. *Polyelectrolytes*; Marcel Dekker: New York, 1971.

(76) Ray, J.; Manning, G. S. *Langmuir* **1994**, *10*, 2450; Manning, G. S. *Biopolymers* **2003**, *69*, 137.

(77) Deserno, M.; Arnold, A.; Holm, C. *Macromolecules* **2003**, *36*, 249.

(78) (a) Young, M. A.; Jayaram, B.; Beveridge, D. L. *J. Am. Chem. Soc.* **1997**, *119*, 59. (b) Ponomarev, S. Y.; Thayer, K. M.; Beveridge, D. L. *Proc. Natl. Acad. Sci. U.S.A.* **2004**, *101*, 14771. (c) Cheng, Y.; Korolev, N.; Nordenskiold, L. *Nucleic Acids Res.* **2006**, *34*, 686. (d) Beveridge, D. L.; Barreiro, G.; Byun, K. S.; Case, D. A.; Cheatham, T. E., III; Dixit, S. B.; Giudice, E.; Lankas, F.; Lavery, R.; Maddocks, J. H.; Osman, R.; Seibert, E.; Sklenar, H.; Stoll, G.; Thayer, K. M.; Varnai, P.; Young, M. A. *Biophys. J.* **2004**, *87*, 3799. (e) Manning, G. S. *Biophys. J.* **2006**, *90*, 3208. (f) Lyubartsev, A. In *Dekker Encyclopedia of Nanoscience and Nanotechnology*; Schwarz, J. A., Contescu, C. I., Putyera, K., Eds.; Marcel Dekker: New York, 2004; p 2131. (g) Korolev, N.; Lyubartsev, A. P.; Laaksonen, A.; Nordenskiöld, L. *Nucleic Acids Res.* **2003**, *31*, 5971.

(79) (a) Winterhalter, M.; Helfrich, W. *J. Phys. Chem.* **1988**, *92*, 6864. (b) Guttman, G. D.; Andelman, D. *J. Phys. II Fr.* **1993**, *3*, 1411.

(80) (a) Safran, S. A.; Pincus, P.; Andelman, D. *Science* **1990**, *248*, 354. (b) Gompper, G.; Goos, J. *J. Phys. II Fr.* **1993**, *3*, 1411.